Molecular Therapy
Original Article

Oral Gavage of Ginger Nanoparticle-Derived Lipid Vectors Carrying Dmt1 siRNA Blunts Iron Loading in Murine Hereditary Hemochromatosis

Xiaoyu Wang,[1] Mingzhen Zhang,[3,4] Shireen R.L. Flores,[1] Regina R. Woloshun,[1] Chunhua Yang,[4] Liangjie Yin,[2] Ping Xiang,[1,6] Xiaodong Xu,[2] Michael D. Garrick,[7] Sadasivan Vidyasagar,[2] Didier Merlin,[4,5] and James F. Collins[1]

[1]Food Science & Human Nutrition Department, University of Florida, Gainesville, FL, USA; [2]Department of Radiation Oncology, University of Florida, Gainesville, FL, USA; [3]Institute of Medical Engineering, School of Basic Medical Science, Health Science Center, Xi'an Jiaotong University, Xi'an, China; [4]Center for Diagnostics and Therapeutics, Institute for Biomedical Science, Georgia State University, Atlanta, GA, USA; [5]Atlanta Veterans Affairs Medical Center, Decatur, GA, USA; [6]State Key Lab of Pollution Control and Resource Reuse, School of the Environment, Nanjing University, Nanjing, China; [7]Department of Biochemistry, State University of New York (SUNY), Buffalo, NY, USA

Nanoparticles (NPs) have been utilized to deliver drugs to the intestinal epithelium *in vivo*. Moreover, NPs derived from edible plants are less toxic than synthetic NPs. Here, we utilized ginger NP-derived lipid vectors (GDLVs) in a proof-of-concept investigation to test the hypothesis that inhibiting expression of divalent metal-ion transporter 1 (Dmt1) would attenuate iron loading in a mouse model of hereditary hemochromatosis (HH). Initial experiments using duodenal epithelial organ cultures from intestine-specific Dmt1 knockout (KO) ($Dmt1^{int/int}$) mice in the Ussing chamber established that Dmt1 is the only active iron importer during iron-deficiency anemia. Further, when $Dmt1^{int/int}$ mice were crossed with mice lacking the iron-regulatory hormone, hepcidin ($Hepc^{-/-}$), iron loading was abolished. Hence, intestinal Dmt1 is required for the excessive iron absorption that typifies HH. Additional experiments established a protocol to produce GDLVs carrying functional Dmt1 small interfering RNAs (siRNAs) and to target these gene delivery vehicles to the duodenal epithelium *in vivo* (by incorporating folic acid [FA]). When FA-GDLVs carrying Dmt1 siRNA were administered to weanling $Hepc^{-/-}$ mice for 16 days, intestinal Dmt1 mRNA expression was attenuated and tissue iron accumulation was blunted. Oral delivery of functional siRNAs by FA-GDLVs is a suitable therapeutic approach to mitigate iron loading in murine HH.

INTRODUCTION

Regulation of intestinal iron absorption is critical to maintain systemic iron homeostasis. Dietary iron exists in several molecular forms, with heme and non-heme (or inorganic) iron being predominant. Although heme iron makes up on average 10%–15% of iron intake in omnivorous humans, its higher absorption efficiency allows it to contribute up to 40% of total absorbed iron.[1] Despite this, the processes and proteins that mediate heme iron absorption in humans and other mammals are not understood in detail. The mechanistic details of absorption of the most abundant dietary form of iron (i.e., non-heme) have, however, been clarified recently.[2] First, ferric non-heme iron is reduced by duodenal cytochrome B (and endogenous and dietary factors); then, ferrous iron is transported into enterocytes by divalent metal-ion transporter 1 (DMT1). Ferrous iron may then be utilized in these cells or exported by ferroportin 1 (FPN1), followed by oxidation by hephaestin. Ferric iron then binds to transferrin in the interstitial fluids for delivery to the liver in the portal blood circulation. Hepcidin, the liver-derived, iron-regulatory hormone, modulates intestinal iron absorption by binding to and triggering internalization and degradation of FPN1 in duodenal enterocytes. Iron export from these cells is the rate-limiting step in iron absorption.

The iron import step mediated by Dmt1 is the focus of this investigation. Mice (microcytic anemia [*mk*])[3,4] and rats (Belgrade [*b*])[5,6] expressing a dysfunctional Dmt1 protein and global *Slc11a2* (encoding Dmt1) knockout (KO) mice[7] suffer from severe iron-deficiency anemia (IDA). Elucidating the causes of the iron deficiency in these animal models is complex, because Dmt1 also functions in iron acquisition from transferrin by developing erythrocytes (and other cells),[8] and it may also facilitate iron reabsorption in the renal tubules.[9] To clarify the specific contribution of Dmt1 to total iron flux, mice lacking Dmt1 only in the intestinal epithelium were generated ($Dmt1^{int/int}$).[7] These mice are severely anemic. When the anemia was corrected by iron supplementation, intestinal iron absorption was drastically reduced in these mice.[10] Yet, paradoxically, most mutant animals live to ~7 months of age without iron supplementation. Survival of these mice into mid-adulthood could be because of the existence of other, complementary intestinal iron transport systems. We therefore initially sought to test the hypothesis that additional,

Received 31 July 2018; accepted 8 January 2019;
https://doi.org/10.1016/j.ymthe.2019.01.003.

Correspondence: James F. Collins, Food Science & Human Nutrition Department, FSHN Building, #441A, 572 Newell Drive, University of Florida, Gainesville, FL 32611, USA.
E-mail: jfcollins@ufl.edu

compensatory iron transport mechanisms exist when Dmt1 function is diminished. Accordingly, we optimized the *ex vivo* Ussing chamber technique to investigate intestinal iron transport in duodenal epithelial organ cultures isolated from intestine-specific Dmt1 KO ($Dmt1^{int/int}$) mice and phenotypically normal littermates ($Dmt1^{fl/fl}$). Because $Dmt1^{int/int}$ mice are anemic, and anemia stimulates intestinal iron absorption, controls were phlebotomized prior to experimentation to render the drive for intestinal iron transport equivalent between genotypes.

We next tested the hypothesis that intestinal Dmt1 mediates the excessive iron accumulation in murine hereditary hemochromatosis (HH). Although this possibility has been experimentally considered by previous investigators, definitive studies have not been reported to date. For example, HFE mice, which model the most common form of human HH,[11] did not load iron when they carried an inactivating mutation in *Slc11a2* (in *mk* mice) or when they were crossed with global *Slc11a2* KO mice.[7,12] Based upon these observations, the authors suggested that impaired intestinal iron absorption explained the lack of an iron-overload phenotype; surprisingly, though, intestinal iron transport was not quantified. This omission is of concern because Dmt1 is expressed in several cell types and has multiple iron-related functions, making interpretation of the data in these studies challenging. Our experimental approach here was designed to eliminate the potential confounding influence of Dmt1 function in other organs by studying mice lacking Dmt1 only in the intestine. We also used a different model of HH, hepcidin KO mice, which represent early-onset (i.e., juvenile) iron loading in humans.[13] Although mutations in *Hamp* (encoding hepcidin) represent a rare cause of HH in humans,[14] observations in this most severe iron-loading condition should be applicable to other (less severe) forms of the disease. The iron-overload phenotype was thus assessed in hepcidin KO mice with and without intestinal Dmt1 function intact.

The final set of experiments was designed to test the hypothesis that blunting intestinal Dmt1 expression and activity will mitigate iron loading in murine HH. A therapeutic approach to inhibit intestinal Dmt1 function *in vivo* was thus developed and tested in hepcidin KO mice. The approach utilized a nanoparticle (NP)-based delivery system that has been used to target hormones, drugs, and small interfering RNAs (siRNAs) to the intestinal epithelium.[15–18] More recently, exosome-like NPs have been isolated from edible plants and utilized to produce NP lipid vectors,[19–22] circumventing some of the toxic properties of synthetic lipid NPs. Here, we utilized ginger NP-derived lipid vectors (GDLVs) to deliver functional Dmt1 (or negative control [NC]) siRNA to the duodenal epithelium of weanling hepcidin KO mice by oral intragastric gavage. After 16 daily treatments, iron loading was assessed using appropriate experimental procedures.

RESULTS

The Ussing Chamber Is Suitable to Quantify Iron Transport in Duodenal Organ Cultures

To determine the optimal dose of ^{59}Fe to be used for Ussing chamber analyses, different doses of ^{59}Fe (15–40 μCi) were initially used in experiments with duodenal epithelial tissues isolated from wild-type (WT) mice. We found that adding 15 μCi of ^{59}Fe to the mucosal side of the chamber was sufficient for detection of radioactivity in the buffer in the opposite chamber (data not shown). We then tested iron transport in duodenum and compared it with mid-jejunum. Results showed that iron flux in the duodenum was substantially higher, with most of the iron transport occurring within 1 h (data not shown). Also, to determine the appropriate concentration of cold Fe substrate ($FeSO_4$) to use, we performed an iron substitution study. The addition of increasing concentrations of $FeSO_4$ (100–2,000 μM) to Ringer's buffer (pH 7.4) revealed the saturation kinetics of Fe Flux (Figure S1). The Michaelis constant (K_m) and maximal rate (V_{max}) were calculated by fitting data to the Hill equation using Origin software (v8.1). The K_m was 540 μM and V_{max} was 7.7 $\mu Eq/cm^2/h$. To ensure that iron transport was functioning near capacity, we used 1,000 μM $FeSO_4$ for subsequent experiments. To define optimal conditions for Fe transport in the Ussing chamber system, we examined buffers with different pHs (Table S1). Buffers were first selected based on their pKa and then tested by acid-base titration. Results showed that Fe flux was significantly higher at pH 6.5 (Figure 1A); therefore, pH 6.5 was used for subsequent analyses. Redoing iron flux measurements at this pH while varying $FeSO_4$ concentrations (100–2,000 μM) (Figure 1B) yielded K_m and V_{max} as 909 μM and 9.6 $\mu Eq/cm^2/h$, respectively. Again, to ensure that iron transport was functioning near capacity, 1,500 μM $FeSO_4$ was used for the remaining experiments.

DMT1 Is the Main Intestinal Iron Importer in Mice

Having established the optimal conditions to quantify iron flux in the Ussing chamber, we next sought to test iron transport activity in $Dmt1^{int/int}$ mice. Daily, for 3 days prior to experimentation, $Dmt1^{fl/fl}$ mice were bled from the facial vein to induce anemia. After phlebotomy, serum hemoglobin (Hb) concentrations were reduced from the normal level (i.e., ~15.0 g/dL) to ~8.5 g/dL in control mice (Figure 1C). This manipulation ensured that the drive for intestinal iron absorption would be similar across genotypes, because $Dmt1^{int/int}$ mice are also anemic (and anemia stimulates iron transport[2]). Experimental results demonstrated that Fe flux was essentially nil for $Dmt1^{int/int}$ mice (Figure 1D). Thus, DMT1 is the predominant duodenal iron importer during anemia.

$Hepc^{-/-}$ Mice Lacking Intestinal DMT1 Grow Slower and Have Enlarged Spleens and Hearts

Hepc KO mice on the C57BL/6 genetic background were backcrossed to mice on the 129S6 genetic background for seven generations, thus producing mice that were >99% congenic for the 129S6 background. $Hepc^{+/-}$ mice were then bred with $Dmt1^{int/+}$ mice (already 129S6 genotype). Littermate male and female mice of four genotypes were subsequently studied ($Hepc^{+/+}/Dmt1^{fl/fl}$, $Hepc^{-/-}/Dmt1^{fl/fl}$, $Hepc^{-/-}/Dmt1^{int/+}$, and $Hepc^{-/-}/Dmt1^{int/int}$). During breeding, we noticed that the $Hepc^{-/-}/Dmt1^{int/int}$ mice were smaller and had pale extremities as adults. At 7 weeks of age, body and liver weights of $Hepc^{-/-}/Dmt1^{int/int}$ mice were decreased with females also exhibiting decreased measures relative to males (Figures 2A and 2B). Also, spleens and hearts were enlarged (Figures 2C and 2D) in the double

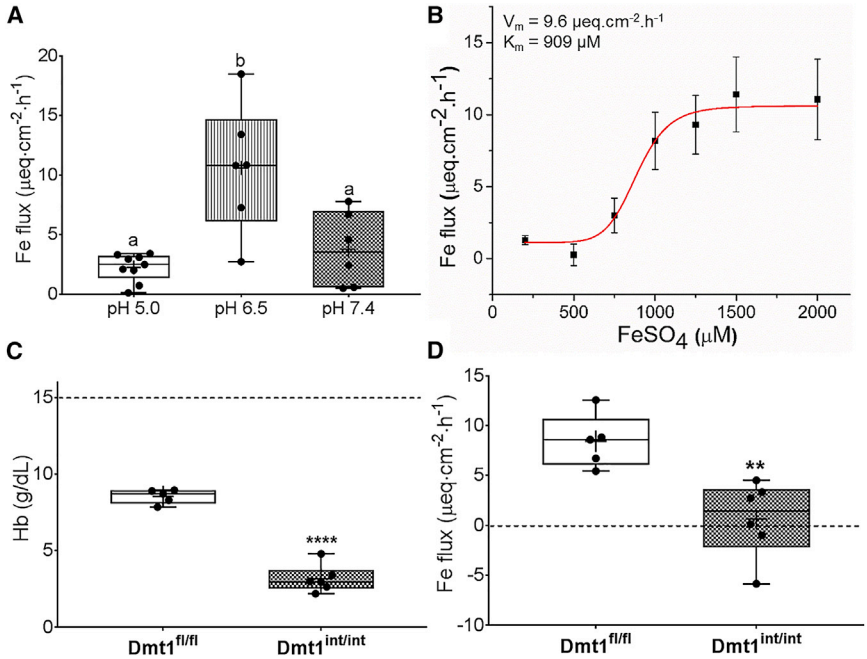

Figure 1. Intestinal DMT1 Is Required for Vectorial Iron Flux across the Duodenal Epithelium during IDA

Duodenal epithelial sheets isolated from adult male WT mice were used initially to determine the optimal conditions for assessing iron flux in the Ussing chamber and then to define kinetic parameters of iron transport. Iron flux was then assessed in anemic adult $Dmt1^{fl/fl}$ and $Dmt1^{int/int}$ mice. Shown is iron (^{59}Fe) flux at pH 5.0. 6.5, and 7.4 in WT mice in the presence of 1,000 µM $FeSO_4$ (n = 6–9 mice/pH group) (A). Iron flux at different iron concentrations (at pH 6.5) in WT mice (n = 3–5 at each iron concentration) was subsequently measured (B), and kinetic parameters were calculated (see values in the upper left corner). Serum Hb concentrations in $Dmt1^{fl/fl}$ mice with facial vein bleeding and untreated $Dmt1^{int/int}$ mice are also shown (n = 5–6/group) (C). The dashed line indicates the approximate Hb concentration in untreated $Dmt1^{fl/fl}$ mice (for comparison). Iron flux was assessed in duodenal sheets isolated from these mice in the presence of 1,500 µM $FeSO_4$ at pH 6.5 (n = 5–6 per group) (D). p = 0.345 for Fe flux being >0 in $Dmt1^{int/int}$ mice. Data were analyzed by one-way ANOVA (A) or t tests (C and D) and are presented as boxplots. Groups labeled with different letters are different from one another: (p = 0.0005) (A); ****p < 0.0001 (C); **p < 0.01 (D).

KOs, but no difference was noted between sexes for these parameters. Overall, these data exemplified impaired growth and alterations in organ weights in $Hepc^{-/-}$ mice lacking intestinal DMT1. These pathological perturbations are consistent with severe iron deficiency.

Intestine-Specific Ablation of DMT1 Increases Erythropoietic Demand in Hepc KO Mice

Blood Hb and hematocrit (Hct) levels in adult $Hepc^{-/-}/Dmt1^{int/int}$ mice were significantly lower than in the other genotypes, but there was no difference between sexes (Figures 3A and 3B). In plasma, total iron-binding capacity (TIBC) was higher in $Hepc^{-/-}/Dmt1^{int/int}$ mice, whereas transferrin saturation (TSAT) was drastically reduced (Figures 3C and 3D). Again, no sex differences were noted for these parameters. Furthermore, renal erythropoietin (EPO) mRNA and protein levels increased, and bone marrow erythroferrone (Erfe) mRNA expression was elevated in $Hepc^{-/-}/Dmt1^{int/int}$ mice (Figures 3E–3G), which is indicative of increased erythropoietic demand.[23] Collectively, these observations demonstrate that intestinal DMT1 is required to prevent the development of anemia in $Hepc^{-/-}$ mice.

Iron Loading Was Abolished in $Hepc^{-/-}$ Mice Lacking Intestinal DMT1

Tissue iron overload occurs in $Hepc^{-/-}$ mice because intestinal iron absorption is inappropriately elevated.[24] While non-heme iron content was significantly increased in serum and all tissues tested in Hepc KO mice (as expected), lack of intestinal DMT1 prevented tissue iron accumulation in double-KO mice (Figures 4A–4E). Moreover, in the spleen, iron was depleted in all $Hepc^{-/-}$ mice, irrespective of whether they expressed functional intestinal DMT1 (Figure 4F). This was expected because it is well established that lack of Hepc leads to splenic iron depletion (from macrophages) because of high FPN1-mediated, iron-export activity.[24] Iron loading in Hepc KO mice thus requires intestinal Dmt1.

Characterization of Ginger-Derived NPs and NP Lipid Vectors

Consistent with a previously published method of isolating and purifying ginger-derived NPs (GDNPs),[25] NPs from the 30%–45% interface of the sucrose gradient were identified as GDNPs (Figure 5A). The average GDNP size was 202.3 nm, as determined by dynamic light scattering (DLS) (Figure 5B). The spherical shape and size of GDNPs were confirmed by transmission electron microscopy (TEM) and atomic force microscopy (AFM) (Figures 5C and 5D). The lipid profile of GDNPs was as follows: 45.1% phosphatidic acid (PA), 29.8% monogalactosyldiacylglycerol (MGDG), 15.6% digalactosyldiacylglycerol (DGDG), and other lipids in smaller amounts (Figure 5E). Lipids extracted from GDNPs spontaneously assemble into GDLVs, as previously described.[16] The average size of GDLVs was 179.3 nm, as determined by DLS (Figure S2A). GDLVs were further confirmed to be nanosized and spheroid when visualized by TEM and AFM (Figures S2B and S2C).

GDLVs Are Non-toxic to Cultured Intestinal Epithelial Cells

Synthetic liposomes or lipid NPs can be toxic when used *in vivo* or *in vitro*. To test the biocompatibility of GDLVs, the MTT assay was first used to measure viability of mouse Colon-26 cells after 24- and 48-h exposure to GDLVs or DC-Chol/DOPE (a synthetic liposome preparation used as a control). This experiment showed that GDLV exposure had minimal effects on the viability of Colon-26 cells, as compared with DC-Chol/DOPE, which showed notable toxicity at both time points (Figure S3A). Second, we monitored barrier function

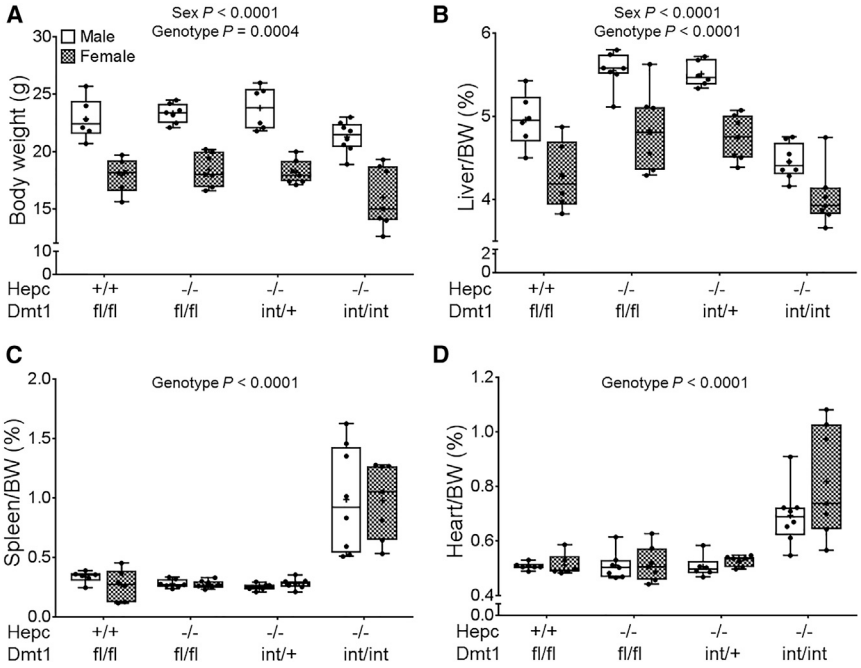

Figure 2. Ablation of Intestinal DMT1 in Hepc$^{-/-}$ Mice Causes Reductions in Body and Liver Weights and Increases in Spleen and Heart Weights

Body and organ weights were assessed in Hepc$^{+/+}$/Dmt1$^{fl/fl}$, Hepc$^{-/-}$/Dmt1$^{fl/fl}$, Hepc$^{-/-}$/Dmt1$^{int/+}$, and Hepc$^{-/-}$/Dmt1$^{int/int}$ mice (male and female littermates) at 7 weeks of age. Shown are body weight (A) and relative liver (B), spleen (C), and heart (D) weights. Data were analyzed by two-way ANOVA and are presented as boxplots for n = 6–8 mice. Data shown in (C) and (D) were $\log_{10}$ transformed because of unequal variance before performing statistical analyses.

of Caco2-BBE human colorectal cancer cells by electrical cell-substrate impedance sensing (ECIS). After cells formed an intact monolayer, 100 μM GDLVs or DC-Chol/DOPE (or PBS as a control) was added to the culture media, and transepithelial electrical resistance (TEER) was measured. TEER was unaffected by GDLV exposure (i.e., similar to control), whereas it significantly decreased in cells exposed to DC-Chol/DOPE (Figure S3B). GDLVs are thus biocompatible with cultured mouse and human intestinal epithelial cells, providing an impetus for *in vivo* testing (as described below).

GDLVs Mediate Uptake of Functional Dmt1 siRNAs into Murine Intestinal Epithelial Cells

After exposing Colon-26 cells to GDLVs or GDLVs loaded with fluorescein isothiocyanate (FITC)-tagged siRNA (green) for 6 h, cells were stained with DAPI (blue) for visualization of nuclei and with phalloidin-tetramethylrhodamine (TRITC) (red) for actin. Confocal microscopic imaging revealed that green dots (siRNA labeled with FITC [siRNA-FITC]) were present inside the GDLVs-siRNA-treated cells (Figure 6A), but not in cells treated with empty GDLVs. Colon-26 cells were also treated with GDLVs-siRNA-FITC (10 and 20 nM) to assess cellular uptake of siRNAs by flow cytometry. The cell uptake efficiency increased from 2 to 6 h and reached more than 50% at both concentrations (Figure S4). Furthermore, to identify a functional Dmt1 siRNA, we used HEK293 cells that overexpressed mouse DMT1 when treated with Dox.[26] Three different commercial Dmt1 siRNAs were tested. Dmt1 siRNA s70783 from Life Technologies showed the maximal knockdown percentage at ~65% (Figure 6B) (data not shown for other siRNAs). To determine whether GDLVs can effectively deliver this functional Dmt1 siRNA into the cell cytoplasm, we incubated HEK293 and Colon-26 cells with Dmt1 siRNA-loaded GDLVs or Dmt1 siRNA-Lipofectamine for 48 h. In Colon-26 cells, both approaches decreased Dmt1 mRNA expression by ~75%, as compared with NC siRNA-transfected cells (Figure 6B). In HEK293 cells, after treatment with Dox, Dmt1 mRNA expression increased about 17-fold in cells treated with NC-siRNA compared with control cells (i.e., not exposed to Dox). Dmt1 mRNA expression decreased ~65% compared with NC-siRNA in the presence of Dox, after treatment with Dmt1 siRNA delivered by GDLVs or Lipofectamine (Figure 6C). These observations proved that GDLVs can deliver Dmt1 siRNA into cells *in vitro* and effectively knock down Dmt1 expression. This finding provided additional justification for *in vivo* experimentation.

FA-GDLVs Have Similar Biochemical Properties to GDLVs and Effectively Target the Duodenum *In Vivo*

Our aim was *in vivo* delivery of functional Dmt1 siRNA to epithelial cells of the duodenum and proximal jejunum, where intestinal iron absorption predominantly occurs (and where DMT1 is most highly expressed). Because GDLVs have been previously shown to mainly target the distal small intestine and colon,[16,25] we considered experimental approaches to more effectively target the proximal small intestine. The B vitamin folate is absorbed in the duodenum and jejunum by the proton-coupled folate transporter (PCFT),[27] and the supplemental form of folate, folic acid (FA), has been used for enhancing NP absorption and bioavailability.[28] We thus produced FA-GDLVs and then experimentally analyzed them to determine whether they had similar biophysical properties to GDLVs. We first demonstrated that, like GDLVs, FA-GDLVs formed a stable complex with siRNAs and protected them from degradation by RNase (Figure S5). Moreover, the size and zeta potential of FA-GDLVs and GDLVs, as assessed by DLS, was almost identical (Figure S6). Biocompatibility of FA-GDLVs and GDLVs was also very similar in that FA-GDLV exposure did not affect growth or proliferation of Colon-26 cells, as determined by MTT assay (Figure S7).

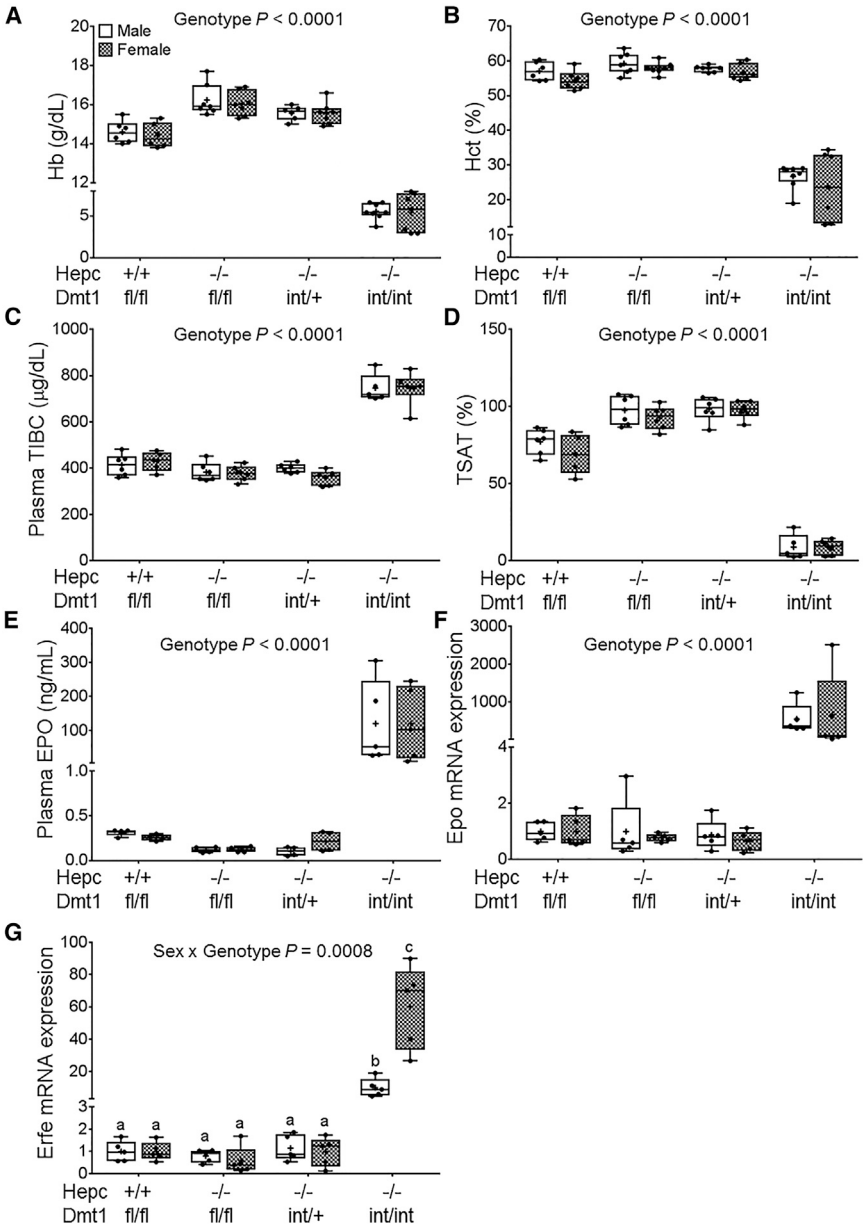

Figure 3. Hepc$^{-/-}$ Mice Develop Severe Anemia When Intestinal Dmt1 Is Ablated

Hematological parameters and biomarkers of erythropoietic demand were assessed in Hepc$^{+/+}$/Dmt1$^{fl/fl}$, Hepc$^{-/-}$/Dmt1$^{fl/fl}$, Hepc$^{-/-}$/Dmt1$^{int/+}$, and Hepc$^{-/-}$/Dmt1$^{int/int}$ mice (male and female littermates) at 7 weeks of age. Shown are Hb (A) and Hct (B) levels in whole blood. Plasma TIBC (C), TSAT (D), and plasma EPO protein levels (E) are also shown. Renal *Epo* (F) and bone marrow *Erfe* (G) mRNA expression was quantified by qRT-PCR. Data were analyzed by two-way ANOVA and are presented as boxplots for n = 6–8 (A and B) or 5–6 (C–G) mice/group. Groups labeled with different letters are different from one another (G). Data shown in (A), (B), and (E)–(G) were $\log_{10}$ transformed because of unequal variance before statistical analyses were performed.

We then administered fluorescent-tagged FA-GDLVs, or GDLVs for comparison, to live mice. Oral gavage of DiIC18(7) (1,1'-dioctadecyl-3,3,3',3'-tetramethylindotricarbocyanine iodide) (DiR)-labeled FA-GDLVs (or GDLVs) to adult mice and subsequent imaging of the duodenum revealed that FA-GDLVs had enhanced retention in the duodenal epithelium (as compared with GDLVs) (Figure 7A). This approach was thus successful at targeting the duodenal epithelium in live mice. Importantly, we also assessed fluorescence in other tissues to determine whether FA-GDLVs escaped the gut. No fluorescence was detected in heart, spleen, lung, liver, or kidney (Figure S8), demonstrating that orally delivered FA-GDLVs do not enter the portal blood circulation or lymph system.

Both Sexes of Hepc KO Mice Begin Loading Hepatic Iron at 2–3 Weeks of Age

Next, because we sought to block iron loading preemptively in this mouse model of severe HH, the time course for iron loading in Hepc$^{-/-}$ mice had to be established to determine when the therapeutic intervention should begin. We therefore characterized the iron loading pattern in male and female Hepc$^{-/-}$ mice at different ages. Results showed that iron began accumulating in the liver between 2 and 3 weeks of age in both sexes (Figure 7B), consistent with considering this mouse mutant a model for juvenile HH. Given the similar, early chronology of iron loading in both sexes, we randomly chose females for further investigation.

FA-GDLVs-Dmt1 siRNA Treatment Does Not Alter Erythropoietic Biomarkers or Cause Inflammation

Prior to assessing the ability of FA-GDLVs to deliver functional Dmt1 siRNA *in vivo*, we sought to assess possible negative physiological outcomes associated with FA-GDLV administration. Serum Hb concentrations, Hct levels, and tissue weights were unaffected by FA-GDLV exposure (Figure S9). Bone marrow *Erfe* and *Tfr1* mRNA expression was also unaltered, suggesting that erythropoietic demand and bone marrow iron levels were unaffected by the treatment (Figures S10C and S10D). Moreover, because serum ferritin is an acute-phase reactant known to be induced by proinflammatory cytokines,[29] and serum ferritin levels did not increase in treated mice (Figure 8B), an inflammatory response likely did not occur. Supporting this inference, there was no change in *TNF-α* and *IL-6* mRNA expression in the liver (Figures S10A and S10B), or myeloperoxidase (MPO) activity in the duodenal epithelium (Figure S11).

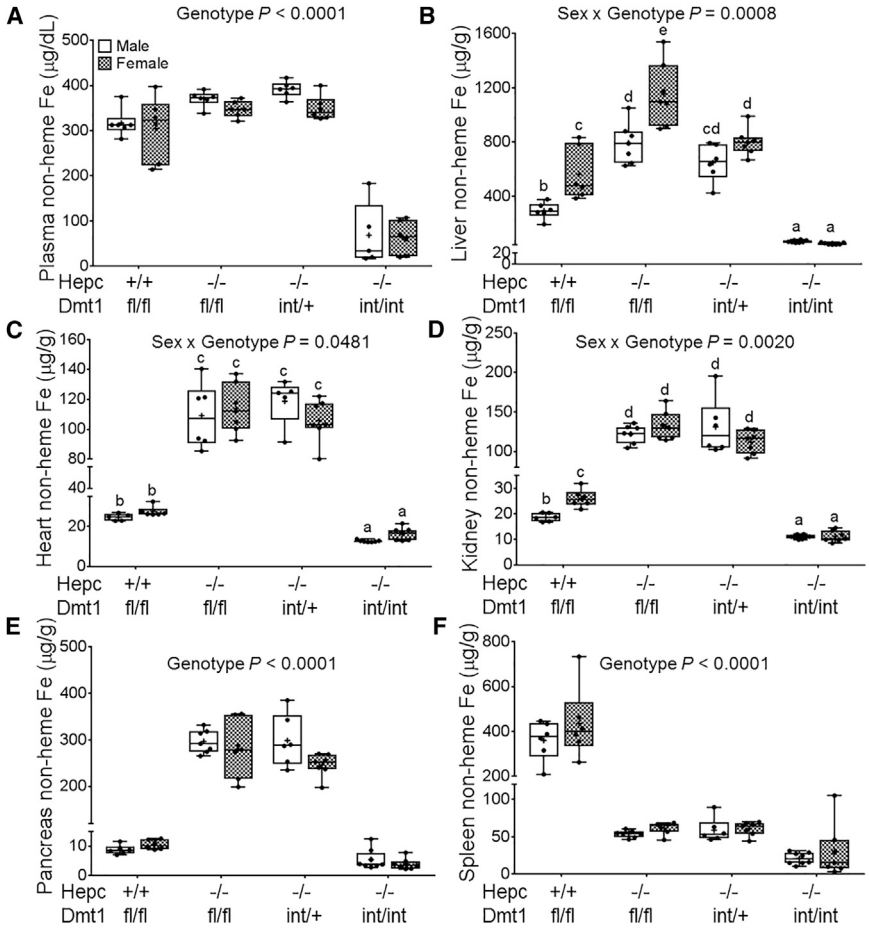

Figure 4. Lack of Intestinal DMT1 Prevents Iron Accumulation in Plasma and Tissues of Hepc$^{-/-}$ Mice

Non-heme iron levels were assessed in Hepc$^{+/+}$/Dmt1$^{fl/fl}$, Hepc$^{-/-}$/Dmt1$^{fl/fl}$, Hepc$^{-/-}$/Dmt1$^{int/+}$, and Hepc$^{-/-}$/Dmt1$^{int/int}$ mice (male and female littermates) at 7 weeks of age. Shown are non-heme iron levels in plasma (A), liver (B), heart (C), kidney (D), pancreas (E), and spleen (F). Data were analyzed by two-way ANOVA and are presented as boxplots for n = 6–8 mice/group. Groups labeled with different letters are different from one another (B–D). Data shown in (B)–(F) were $\log_{10}$ transformed because of unequal variance before statistical analyses were performed.

FA-GDLVs-Dmt1 siRNA Administration Specifically Downregulated Dmt1 mRNA Expression in the Duodenal Epithelium and Mitigated Iron Loading in Hepc KO Mice

Because iron loading begins in neonates, we started the treatment at 19 days of age, just prior to weaning. Dmt1 mRNA expression decreased by ~50% in the duodenal epithelium 24 h after oral administration of Dmt1 siRNA-loaded FA-GDLVs (as compared with NC siRNA-loaded FA-GDLVs) (Figure 8A). The treatment did not, however, affect hepatic, renal, or bone marrow Dmt1 mRNA expression (Figure S12), demonstrating specificity for the intestinal epithelium. Serum ferritin levels decreased ~40% in mice treated with Dmt1 siRNA-loaded GDLVs compared with NC-siRNA, demonstrating that body iron load decreased (Figure 8B).[30] In support of this contention, serum non-heme iron and TSAT were reduced, and non-heme iron content was significantly lower in the liver, kidney, pancreas, and heart of mice treated with Dmt1 siRNA-loaded FA-GDLVs (Figures 8C–8H). Collectively, these data provide proof-of-concept that: (1) Dmt1 is a suitable therapeutic target to blunt iron loading in HH; and (2) oral administration of an experimentally verified, functional Dmt1 siRNA by FA-GDLVs is a suitable treatment approach to mitigate iron loading in mouse models of genetic iron overload.

DISCUSSION

Iron homeostasis in mammals depends critically on Dmt1, because it is required for optimal assimilation of dietary iron in the gut and acquisition of transferrin-bound iron by developing erythrocytes. Dmt1 may also function in iron reabsorption from the renal filtrate.[9,31–33] Perturbations in any of these physiological processes could disrupt systemic iron homeostasis. Humans harboring inactivating Dmt1 mutations are severely anemic,[34–40] but the relative contributions of the different Dmt1 functions to the disease phenotype have not been established definitively. Mice and rats carrying an identical point mutation in the *Slc11a2* gene,[4,6] and global *Slc11a2* KO mice,[7] all have very similar iron-deficient phenotypes; but similarly, how impairments in intestinal iron absorption, iron delivery to the erythron, and renal iron reabsorption contribute quantitatively to the noted IDA is unclear.

Dmt1$^{int/int}$ Mice Acquire Sufficient Iron to Support Growth and Development into Mid-adulthood

Mice lacking Dmt1 specifically in the intestinal epithelium develop severe IDA.[7] Iron-supplemented Dmt$^{int/int}$ mice (with normal hematological parameters) assimilated <15% of the iron dose absorbed by control mice.[10] The magnitude of iron absorption in untreated (anemic) Dmt$^{int/int}$ mice has, however, not been experimentally assessed. The need to understand the contribution of intestinal Dmt1 to total iron transport made it important to perform absorption studies in Dmt$^{int/int}$ mice with no other interventions because the drive for iron absorption increases in IDA (with concurrent hypoxia), and mechanisms of iron absorption could be quite different under these circumstances. This understanding is especially important given that these mice acquire enough iron to support growth and maturation into mid-adulthood (unpublished data)[10] in the absence of intestinal Dmt1. So, the pertinent question here is: how do these mice acquire sufficient iron to survive to 6–7 months of age? Three logical

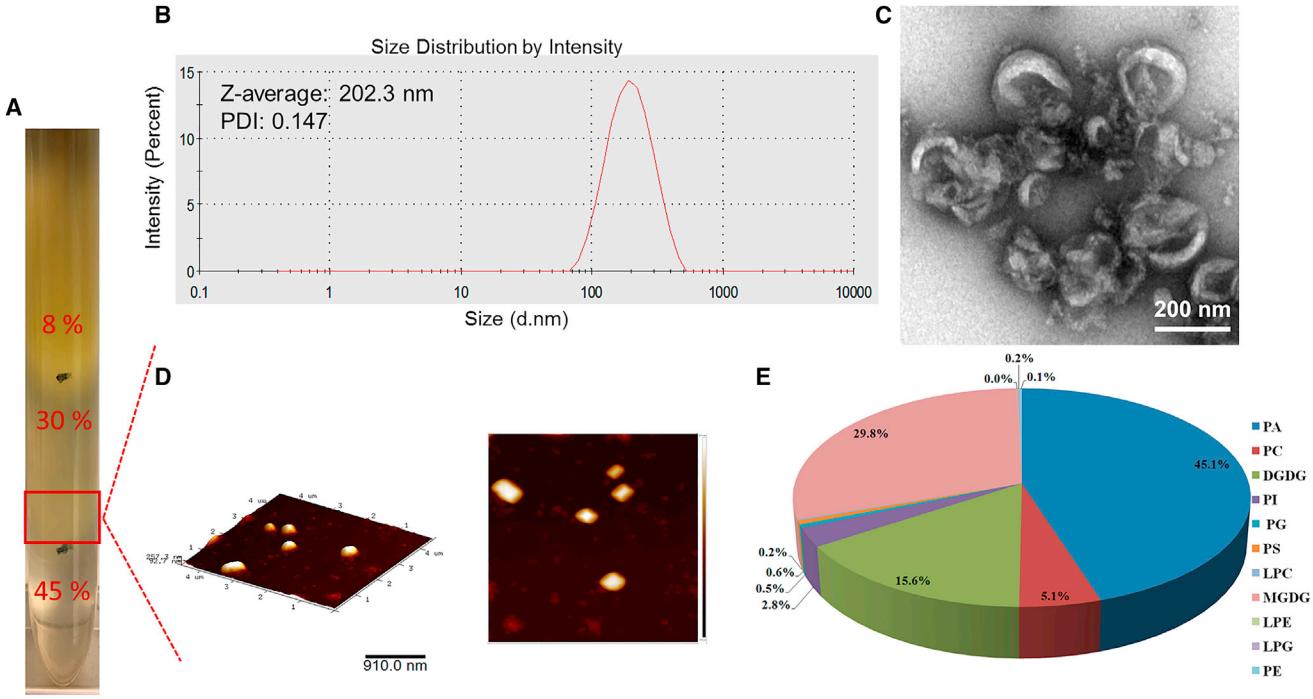

Figure 5. Characterization of Ginger-Derived Nanoparticles

Three bands were formed after step sucrose gradient ultracentrifugation (A); GDNPs from 30%/45% interface were measured by dynamic light scattering (DLS) (B) and visualized by transmission electron microscopy (TEM) (C) and atomic force microscopy (AFM) (D). Also shown is the lipid profile of GDNPs (n = 5) (E). DGDG, digalactosyldiacylglycerol; LPC, lysophosphatidylcholine; LPE, lysophosphatidylethanolamine; LPG, lysophosphatidylglycerol; MGDG, monogalactosyldiacylglycerol; PA, phosphatidic acid; PC, phosphatidylcholine; PE, phosphatidylethanolamine; PG, phosphatidylglycerol; PI, phosphatidylinositol; PS, phosphatidylserine.

possibilities come to mind. First, perhaps Dmt$^{int/int}$ mice are born with a sufficient iron endowment to live to this age in the absence of any significant absorption of dietary iron. Sole reliance on stores, however, seems unlikely because mice normally meet ~50% of iron requirements from the diet,[41,42] with the other 50% presumably coming from iron recycling. Second, because the villin-Cre transgene may show a mosaic expression pattern in the intestinal epithelium, residual Dmt1 iron-transport activity could preserve life in these mice. Previous investigations, however, have not detected Dmt1 expression in the intestinal epithelium of these mice.[7] And last, another transport process could provide adequate iron absorption capacity to prevent earlier mortality. This is a realistic possibility because, for example, some Zip transporters can transport iron[43,44] and some are expressed in the intestine.[45] Here, we thus sought to test the hypothesis that another dietary iron transport process exists in the proximal small intestine of Dmt$^{int/int}$ mice.

Dmt1 Is the Principal Intestinal Iron Importer during IDA

We established the Ussing chamber technique to define mechanisms of intestinal iron transport and to determine the relative contribution of Dmt1 to intestinal iron flux. This *ex vivo* technique has provided novel insights into many intestinal transport processes.[46] A principal strength of this approach is that it provides a short-term organ culture method that enables precise measurement of electrical and transport parameters of intact, polarized intestinal epithelium. After defining the optimal transport conditions and defining the kinetics of iron flux, we applied this technique to duodenal epithelial organ cultures isolated from control and Dmt1$^{int/int}$ mice. These experiments demonstrated that Dmt1 is required for the enhancement of intestinal iron transport associated with IDA. This finding complements and extends the previous observation that Dmt1 is the principal intestinal iron importer during physiological conditions in these mice.[10] That Dmt1$^{int/int}$ mice live for several months may thus relate to compensatory mechanisms that decrease iron losses, given that iron excretion may play an important role in systemic iron homeostasis in mice.[42] Alternatively, Dmt1-independent iron import processes could be active in more distal portions of the gastrointestinal (GI) tract in these mice.

Intestinal Dmt1 Mediates the Excessive Iron Absorption that Typifies Murine HH

Recent studies also suggested that Dmt1 was the main iron entry pathway in murine HH. This prediction was based upon the facts that when a mouse model of adult-onset HH, the HFE KO mouse, was bred to *mk* mice (expressing dysfunctional Dmt1)[4] or global *Slc11a2* Kos,[7] tissue iron accumulation was prevented.[7,12] Interpretation of these data is, however, complicated by the fact that, as mentioned above, Dmt1 is expressed in multiple tissues and cell types, and has multiple notable physiologic functions. Importantly,

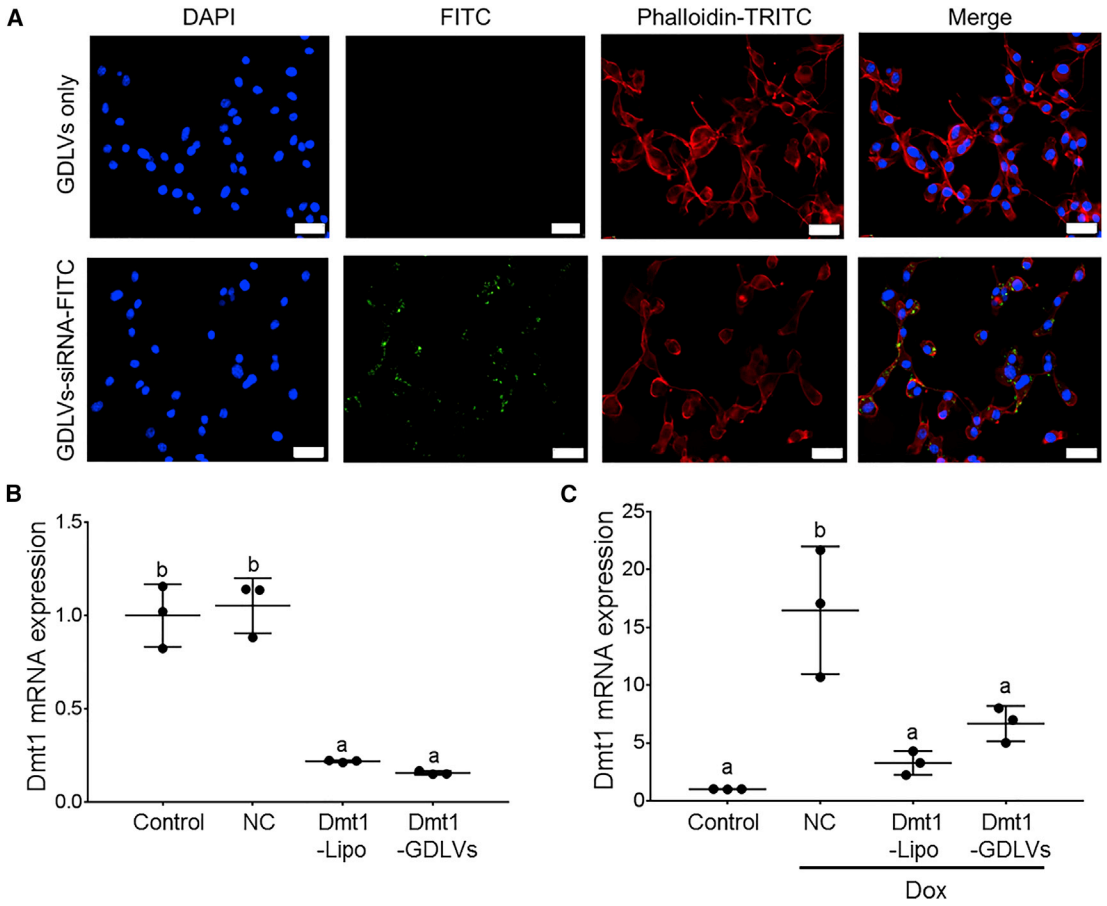

Figure 6. Ginger Nanoparticle-Derived Lipid Vectors Effectively Deliver siRNAs into Colon-26 and HEK293 Cells

Colon-26 cells were treated with GDLVs only or with GDLVs carrying FITC-labeled (control) siRNAs (green) for 6 h and then processed for confocal microscopy (A). Fixed cells were stained with DAPI (blue) for visualization of nuclei and with phalloidin-TRITC (red) for actin. Colon-26 (B) and Dmt1-overexpressing HEK293 cells (C) were untreated (control) or were transfected with NC- or Dmt1-siRNAs delivered by Lipofectamine (Dmt1-Lipo) or GDLVs (Dmt1-GDLVs). Dmt1 mRNA expression was subsequently assessed in the cells by qRT-PCR. Data were analyzed by one-way ANOVA and are presented as mean ± SD for n = 3 individual experiments. Groups labeled with different letters are different from one another ($p < 0.0001$). Dox, doxycycline.

intestinal iron transport was not measured in any of these previous investigations. Our goal here was thus to clarify this issue by experimentally defining the specific contribution of intestinal Dmt1 to the excessive iron absorption that typifies murine HH. By using mice lacking Dmt1 only in the intestinal epithelium, we avoided possible confounding influences of Dmt1 in other tissues and organs. Our experimental approach also utilized a model of early-onset (i.e., juvenile) HH, because we postulated that observations made in the most severe form of the disease would be applicable to all other types of (less severe) HH. This is a logical hypothesis because all forms of HH (except for "ferroportin" disease [i.e., type 4 HH]) share similar molecular underpinnings (due to inappropriate hepcidin expression and activity). Importantly, in the current investigation, experiments done with double-KO mice (i.e., hepcidin KO plus lack of intestinal Dmt1) demonstrated that intestinal Dmt1 is required for the iron loading that typifies murine HH. These observations are in agreement with earlier predictions and provide strong rationale for therapeutic targeting of intestinal Dmt1 to mitigate iron loading in HH.

Proof-of-Concept for a Novel Treatment Modality for HH

We next conceptualized, developed, and optimized a new experimental approach to blunt Dmt1 activity *in vivo*. First, a functional Dmt1 siRNA was developed and tested *in vitro*. Next, the GDLV-mediated siRNA delivery system was adapted to target the proximal small bowel (by incorporating FA). We subsequently demonstrated that orally administered FA-GDLVs carrying Dmt1 siRNAs successfully blunted tissue iron accumulation in $Hepc^{-/-}$ mice. Importantly, we found no evidence of inflammation or toxicity associated with FA-GDLVs administration, or off-target effects on Dmt1 expression in other tissues. The experimental approach utilized here thus represents a novel intervention to mitigate iron loading in murine HH. It also seems likely that this approach could be adapted to treat humans with HH, and possibly other iron-loading disorders including, for

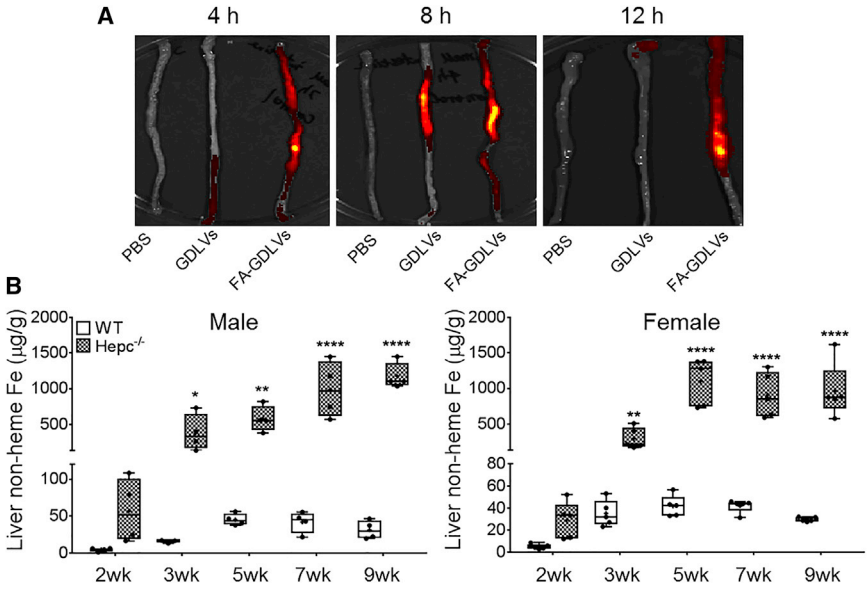

Figure 7. Oral Administration of FA-GDLVs Targeted the Upper GI Tract and Time Course of Iron Loading in Hepc$^{-/-}$ Mice

Six-week-old male mice were administered PBS, fluorescent-tagged GDLVs, or fluorescent-tagged FA-GDLVs by oral intragastric gavage. The proximal small bowel was imaged 4, 8, and 12 h after administration (the duodenum is at the top of the pictures) (A). Liver non-heme iron content was measured in both sexes of WT and Hepc$^{-/-}$ mice at different ages (2–9 weeks) (B). Data were analyzed by one-way ANOVA and are presented as boxplots for n = 4–5 mice/group. *p < 0.05; **p < 0.01; ****p < 0.0001, indicating differences as compared with WT mice at each age. FA, folic acid.

example, β-thalassemia. This is important because existing treatment modalities for iron overload in humans are either not specific for iron (repeat phlebotomies) or have significant side effects (use of oral iron chelators). Oral administration of FA-GDLVs carrying siRNAs targeting iron transporters (e.g., Dmt1 or Fpn1) could thus serve as an alternative therapeutic strategy to attenuate iron absorption, while avoiding some negative outcomes associated with currently used treatment regimens. Moreover, although here we demonstrated successful prevention of iron loading during the early stages of disease pathogenesis, we predict that this therapeutic approach could also reverse iron accumulation once established, especially if utilized in conjunction with iron removal by phlebotomy or chelation.

One limitation of this investigation is the use of laboratory mice, which cannot efficiently utilize heme iron, whereas omnivorous humans derive a significant portion of body iron from dietary heme (up to ≈40%). Heme is probably taken up into enterocytes via endocytosis, and the heme may then be degraded by heme oxygenase, releasing free iron into the lumen of the endosome. It is possible that Dmt1 then transports this iron out of endosomes into the cytosol for utilization by the cell or export via Fpn1. This would be analogous to the function of Dmt1 in the assimilation of transferrin-bound iron by developing erythrocytes. Because much of what we know about iron homeostasis in mammals comes from studies in mice, whether intestinal Dmt1 functions in the assimilation of diet-derived heme iron is, unfortunately, unknown (since mice cannot absorb heme iron). Moreover, it is not clear whether enhanced absorption of heme iron contributes to the development of iron overload in HH in humans; some studies support this possibility,[47] and others do not.[48] Nonetheless, because iron absorption is only marginally enhanced in humans with HH (from 1–2 mg/day up to ≈4 mg/day),[49] silencing Dmt1, even if it only blunts non-heme iron absorption, should be effective at reducing body iron burden over time.

MATERIALS AND METHODS

Mouse Models and Breeding Strategy

All animal studies were approved by the University of Florida Institutional Animal Care and Use Committee (IACUC). Intestine-specific Dmt1 KO (Dmt1$^{int/int}$) mice and phenotypically normal (Dmt1$^{fl/fl}$) control littermates[7] and Hepc KO (Hepc$^{-/-}$) mice[24] were utilized for this investigation. The goal was to produce mice with intestine-specific Dmt1 KO plus (iron overload due to) Hepc KO. Mice with floxed Dmt1 and a villin-Cre transgene lose Dmt1 in an intestine-specific fashion (DMT1$^{int/int}$), whereas those lacking the villin-Cre (DMT1$^{flox/flox}$) serve as phenotypically normal controls. We obtained these mice from Dr. Bryan Mackenzie at the University of Cincinnati on the 129S6 inbred background (also note that these mice were originally derived from the laboratory of Dr. Nancy Andrews). Hepc KO mice on the C56BL/6 background were obtained from Dr. Ella Nemeth at the University of California Los Angeles (also note that these mice were originally derived from the laboratory of Dr. Sophie Vaulont). Hence, we first had to generate Hepc KO mice on the 129S6 background, by breeding Hepc KO mice with WT 129S6 mice for seven generations. Then the following crosses were done to generate control and experimental mice for this investigation:

$$\text{F0: Hepc}^{-/-}|\text{DMT1}^{+/+}|\text{Cre}^{-/-} \times \text{Hepc}^{+/+}|\text{DMT1}^{flox/flox}|\text{Cre}^{+/-}$$

$$\text{F1: Hepc}^{+/-}/\text{DMT1}^{+/fl}/\text{Cre}^{+/-} \times \text{Hepc}^{+/-}/\text{DMT1}^{+/fl}/\text{Cre}^{-/-}$$

$$\text{F2: Hepc}^{+/-}/\text{DMT1}^{fl/fl}/\text{Cre}^{-/-} \times \text{Hepc}^{+/-}/\text{DMT1}^{+/fl}/\text{Cre}^{+/-}.$$

Keeping only these two genotypes from the F2 generation (representing just 1/16 of the progeny) for breeding allowed us to segregate parentals and produce the desired experimentals and controls: Hepc$^{+/+}$/Dmt1$^{fl/fl}$ (normal controls), Hepc$^{-/-}$/Dmt1$^{fl/fl}$ [Hepc KO, normal intestinal Dmt1 expression), Hepc$^{-/-}$/Dmt1$^{int/+}$ (Hepc KO with one copy of the intestinal Dmt1 gene ablated), and Hepc$^{-/-}$/Dmt1$^{int/int}$ (Hepc KO lacking intestinal Dmt1, i.e., double KOs]. Littermate male and female mice of these four genotypes were studied. For some experiments, Dmt1$^{fl/fl}$ mice were bled from the facial vein to

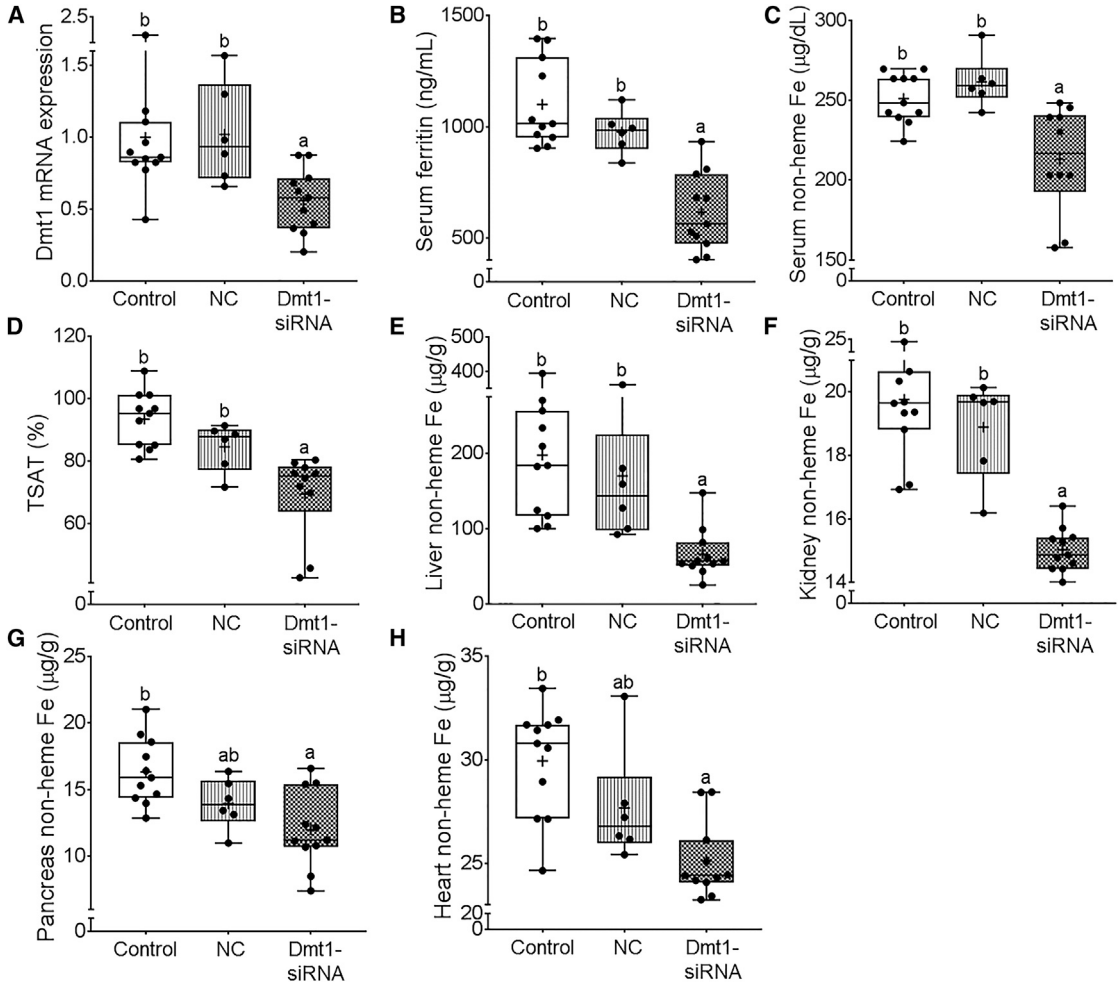

Figure 8. Oral Administration of FA-GDLVs Loaded with DMT1 siRNA Mitigated Iron Loading in Hepc$^{-/-}$ Mice

19-day-old female Hepc$^{-/-}$ mice were orally gavaged with saline (control), negative control-siRNA FA-GDLVs (NC), or Dmt1-siRNA FA-GDLVs daily for 16 days. Mice were provided a standard chow diet on days 1–8 and then a semi-purified, low-iron diet on days 9–16. Shown is *Dmt1* mRNA expression in isolated intestinal epithelial cells (A), serum ferritin concentrations (B), serum non-heme Fe concentrations (C), TSAT (D), and liver (E), kidney (F), pancreas (G), and heart (H) non-heme Fe concentrations. Data were analyzed by one-way ANOVA and are presented as boxplots for n = 6–11 mice/group. Groups labeled with different letters are different from one another: $p < 0.0001$ (A and F); $p = 0.0138$ (B); $p = 0.0007$ (C); $p = 0.0001$ (D); $p = 0.0011$ (E); $p = 0.002$ (G); $p = 0.0003$ (H).

induce anemia (Dmt1$^{int/int}$ mice were similarly handled, but not bled, because they are already anemic).

Measurement of Transepithelial Fe Flux

Fresh duodenal mucosa was mounted between two halves of an Ussing chamber with 0.3 cm^2 of exposed surface area (P2304; Physiologic Instruments, San Diego, CA, USA). For initial experiments, we used Ringer's solution (in mM: 140 Na^+, 119.8 Cl^-, 5.2 K^+, 2.4 HPO_4^{2-}, 0.4 $H_2PO_4^-$, 1.2 Mg^{2+}, 1.2 Ca^{2+}, and 25 HCO_3^- [pH 7.4]).[50] Subsequently, transport buffers at pH 5.0, 6.5, and 7.4 were formulated specifically for Fe flux studies (Table S1). During experiments, buffers were maintained at 37°C and bilaterally infused with a 95% O_2-5% CO_2 gas mixture. $FeSO_4$ was added to Ringer's or transport buffers at 100, 200, 500, 750, 1,000, 1,250, 1,500, and 2,000 µM to define the kinetics of iron transport. Tissues were allowed to stabilize in buffers for 30 min after being placed in the chamber, and Fe flux across the duodenal epithelium was then analyzed by adding ^{59}Fe (in 0.5 M HCl, neutralized with *N*-methyl-D-glucamine) to the mucosal or serosal chamber. Buffer samples were then collected from the opposite chamber every 15 min for 1 h. ^{59}Fe activity in the collected buffers was measured using a gamma counter (Wizard 2, 2480 Automatic Gamma Counter; Perkin Elmer). During the transport assay, basal short-circuit current and conductance were recorded using a computer-controlled voltage and current clamp device (VCC MC-8; Physiologic Instruments), as previously described.[51,52] Unidirectional flux (J) was calculated as J_{ms} (or J_{sm}) (where m is mucosal and s is serosal) = V × (S2 − S1 × dilution)/(specific activity × surface area × time), where V is the volume of sink superfusate (in mL);

S1 and S2 are the cpm of samples taken at the beginning and end of the flux period, respectively; dilution is of the sink superfusate resulting from sample fluid replacement; specific activity is the isotopic activity in the source bath (cpm/μEq); surface area is the area of exposed mucosa; and time is the length of the flux period in hours. Fe flux was calculated as $J_{net} = J_{ms} - J_{sm}$.

Production of GDNP Lipid Vectors for siRNA Delivery

GDNPs were isolated and purified according to established methods.[25] To produce GDLVs, 6 mL of methyl alcohol/chloroform (2:1) (v/v) was added to 1.6 mL of GDNPs (1 mg/mL) in PBS followed by thorough mixing. Next, chloroform (2 mL) and double-distilled H_2O (ddH_2O; 2 mL) were added sequentially and the solution was vortexed. The solution was then centrifuged at 2,000 × *g* for 10 min at room temperature to separate the aqueous and organic phases.[16] To produce FA-GDLVs, 50 μL of FA (F7876; Sigma-Aldrich) (1.5 mg/mL in DMSO) was mixed with total lipids (organic phase), and the solution was dried in a round-bottomed flask to a thin lipid film in a rotary evaporator. The dried lipid layer was then suspended in 500 μL of 4-(2-hydroxyethyl)-1-piperazineethanesulfonic acid (HEPES) buffer (20 mM [pH 7.4]; Sigma-Aldrich). After 5 min of sonication, an equal volume of HEPES buffer was added and the solution was sonicated again for 5 min, finally producing FA-GDLVs.

For siRNA loading of GDLVs and FA-GDLVs, Dmt1- or negative control (NC)-siRNA (3.75 nmol) was dissolved in 300 μL of a sterile 5% glucose solution and vortexed gently. For *in vitro* GDLVs plus siRNA formulation, dried GDLVs (from 1.6 mg GDNPs) were immediately suspended in 500 μL of 20 mM HEPES buffer (pH 7.4), which contained 3.75 nmol DMT1 siRNA. After sonicating for 5 min, an equal volume of HEPES buffer was added and the mixture was sonicated for another 5 min. Finally, the solution was passed through liposomes extruded with a 200-nm polycarbonate membrane about 20 times. For *in vitro* studies, 15 pmol GDLVs/siRNA was added to test the transfection efficiency. TurboFect reagent (Life Technologies) (6 μL) was then added to the diluted siRNA solutions, and the sample was mixed immediately and incubated for 15 min at room temperature. For *in vivo* studies, high-performance liquid chromatography (HPLC)-purified siRNAs were used because they have better stability and less toxicity (than less pure preparations). For the *in vivo* FA-GDLVs/siRNA formulation, DMT1 siRNA (3.75 nmol) was first dissolved in sterile 300 μL 5% glucose solution, vortexed gently, and spun down. Then, TurboFect reagent was added (6 μL) to the diluted siRNA, which was mixed immediately and incubated for 15 min at room temperature. The packed siRNA plus TurboFect was then added to the GDLVs-FA lipid film with sonication to prepare FA-GDLVs/siRNA. For *in vivo* studies, 3.75 nmol GDLVs/siRNA per dose was used to knock down DMT1 expression in duodenum.

Cytotoxicity Assay

The 3-(4,5-dimethylthiazol-2-yl)-2,5-diphenyltetrazolium bromide (MTT) assay was used to analyze cell viability, as previously described.[18] Colon-26 cells were incubated with different concentrations of GDLVs, DC-Chol/DOPE (30/70 mol/mol; Avanti Polar Lipids) (0, 10, 20, 50, 100, 200 μM), or FA-GDLVs for 24 or 48 h. A cell attachment assay was used to observe real-time cytotoxicity by ECIS, as described in a previous study.[18] Caco2-BBE cells were seeded on plates and grown to confluence. Control (PBS), GDLVs or FA-GDLVs (100 μmol/L), or DC-Chol/DOPE (30/70 mol/mol) (100 μmol/L) was added to the wells. Basal electrical resistance measurements were then performed using the ideal parameters for Caco2-BBE cells, 500 Hz and 1 V.

Characterization of GDNPs, GDLVs, and FA-GDLVs

NPs were characterized using TEM (for GDNPs and GDLVs only), AFM, and DLS. Particle size was measured using DLS (Malvern Instruments, Worcestershire, UK) at room temperature. For TEM imaging, one drop of sample was deposited onto the surface of Formvar-coated copper grids, and then 1% uranyl acetate was added for 15 s. Samples were allowed to dry at room temperature before imaging. AFM images were taken using a SPA 400 AFM (Seiko Instruments, Chiba, Japan). Lipid extract from GDNPs was analyzed by the Lipidomics Research Center at Kansas State University.

Cell Culture

HEK293 cells were engineered so that the mouse Dmt1 cDNA was expressed only when cells were treated with doxycycline (Dox; a tetracycline analog).[26] Dmt1-overexpressing HEK293 cells or mouse Colon-26 cells were grown to 60% confluence and then transfected with Dmt1- (s70782, s70783, or s70784; Life Technologies, Gaithersburg, MD, USA) or NC-siRNA (4390843; Life Technologies) using Lipofectamine RNAiMAX (Thermo Fisher Scientific, Fair Lawn, NJ, USA) or GDLVs. Cells were analyzed 48 h later.

Cell Uptake of GDLVs Carrying siRNA Labeled with FITC

For fluorescence imaging of cellular uptake, Colon-26 cells were seeded at 1×10^5 cells/well on eight-chamber slides (Tissue-Tek; Sakura, USA) and cultured overnight at 37°C. Then, the medium was removed, cells were rinsed with PBS, and Opti-MEM containing GDLVs + siRNA-FITC (15 pmol/well) was added. After 8-h incubation at 37°C, cells were rinsed with PBS and fixed with 4% paraformaldehyde for 15 min and then dehydrated with acetone at −20°C for 5 min. After blocking with 1% BSA in PBS for 30 min, 100 μL of phalloidin-TRITC (1:40 dilution; Sigma-Aldrich) was added, and the cells were incubated for an additional 30 min. Finally, cells were coverslip-mounted with mounting medium containing DAPI (H-1500; Vector Laboratories). Cells were then imaged using a fluorescent microscope (BX63; Olympus, Japan). Cell uptake efficiency was quantified by flow cytometry by gating for FITC fluorescence (BD LSR Fortessa flow cytometer; BD Biosciences).

Animal Studies

Mice were anesthetized by CO_2 narcosis and killed by cervical dislocation. Hb and Hct in whole blood were measured by standard methods.[53,54] Serum ferritin concentration was quantified with the Mouse Ferritin ELISA Kit (ab157713; Abcam). Plasma EPO concentration was measured by Mouse Erythropoietin Quantikine ELISA Kit

(MEP00B; R&D Systems). Plasma non-heme iron concentrations were determined using a standard colorimetric method.[54,55] TIBC was assessed as previously described.[53,54] TSAT was calculated as serum iron/TIBC × 100. Non-heme iron content in tissues was determined using a standard acid digestion, chromogen-based colorimetric assay.[53,54]

To evaluate the ability of NPs to target the mouse duodenum *in vivo*, 6-week-old male C57BL/6 mice were fasted for 24 h, and then PBS or DiR dye (PromoKine, Heidelberg, Germany)-labeled GDLVs or FA-GDLVs were administered to mice by oral intragastric gavage. The proximal small intestine was imaged 4, 8, and 12 h later by an IVIS series preclinical *in vivo* imaging system (Perkin Elmer, MA, USA). Subsequently, 19-day-old female WT and Hepc$^{-/-}$ mice were provided PBS (control), freshly made negative control-siRNA (NC-siRNA), or Dmt1-siRNA (3.75 nmol/dose)-loaded FA-GDLVs daily for 16 days by oral intragastric gavage. During the first 8 days, mice were fed a standard chow diet with 200 ppm Fe (#2918; Envigo), but were then switched to a low-iron diet (2–6 ppm Fe; TD.80396; Envigo) for the last 8 days. Because the standard chow diet contained excess iron (i.e., above the approximate 35 ppm requirement for adult mice[56]), we postulated that the low-iron diet would maximize the upregulation of Dmt1 expression, which occurs because of high Fpn expression (because Hepc is absent) and consequent intracellular iron depletion.[57] This approach mimics HFE-related HH,[58] the most common form of the disease in humans, in which Dmt1 expression in enterocytes is abnormally high with normal or low iron intakes. Moreover, given high Dmt1 and Fpn1 expression, and because *in vivo* delivery of anti-Dmt1 siRNA blunted Dmt1 expression by only ≈40%, we postulated that we would be more likely to see an effect when dietary iron intake was low. We also postulated that this experimental approach would nicely mimic humans with HH, because some published reports support the effectiveness of dietary (and supplemental) iron restriction in disease management.[59]

Real-Time qPCR

Total RNA was isolated using RNAzol RT reagent (Molecular Research Center, OH, USA). RNA concentration was measured using a NanoDrop spectrophotometer. SYBR-Green qRT-PCR was performed as described.[60] Expression of experimental genes was normalized to expression of cyclophilin A. Primer sequences are listed in Table S2.

Statistical Analyses

Results are depicted as boxplots displaying the minimum, the lower (25th percentile), the median (50th percentile), the upper (75th percentile), and the maximum ranked sample. The mean values are indicated by a plus (+) sign. In Figures 6B and 6C, data are presented as mean ± SD. Statistical analysis was performed using GraphPad Prism (v 7.0), Stata (v 15.1), or JMP (v 12.2). Data were analyzed by Student's t test or one- or two-way ANOVA followed by a Tukey's multiple comparisons test. The Brown-Forsythe test or Levene's test was used to check for equal variance when one-way or two-ANOVA was used, respectively. Some data were $\log_{10}$ transformed due to unequal distribution (as indicated in the figure legends). Note, however, that the non-transformed data are shown in the figures for ease of visual interpretation. $p < 0.05$ was considered statistically significant.

SUPPLEMENTAL INFORMATION

Supplemental Information includes twelve figures and two tables and can be found with this article online at https://doi.org/10.1016/j.ymthe.2019.01.003.

AUTHOR CONTRIBUTIONS

S.V., M.D.G., D.M., and J.F.C. conceptualized this investigation. X.W., M.Z., S.R.L.F., R.R.W., C.Y., L.Y., P.X., and X.X. performed experiments. X.W., M.Z., M.D.G., S.V., D.M., and J.F.C. designed experiments and interpreted data. X.W. drafted the manuscript, performed statistical analyses, and made the figures. All authors participated in writing the manuscript and approved the final version of the paper.

CONFLICTS OF INTEREST

The authors declare no competing interests.

ACKNOWLEDGMENTS

This investigation was funded by grant R01 DK074867 from the National Institute of Diabetes and Digestive and Kidney Diseases (NIDDK) and grant R01 DK109717 from NIDDK and the Office of Dietary Supplements (to J.F.C.). X.W. is a recipient of a doctoral scholarship from the China Scholarship Council. M.Z. was the recipient of a Research Fellowship Award from the Crohn's & Colitis Foundation of America. D.M. is a recipient of a Senior Research Career Scientist Award from the Department of Veteran Affairs. The authors wish to thank Dr. Bryan McKenzie for providing the Dmt1$^{int/int}$ mice, Drs. Sophie Vaulont and Ella Nemeth for providing the Hepc$^{-/-}$ mice, and Dr. Laura Garrick for critical reading of the manuscript.

REFERENCES

1. Hurrell, R., and Egli, I. (2010). Iron bioavailability and dietary reference values. Am. J. Clin. Nutr. *91*, 1461S–1467S.

2. Gulec, S., Anderson, G.J., and Collins, J.F. (2014). Mechanistic and regulatory aspects of intestinal iron absorption. Am. J. Physiol. Gastrointest. Liver Physiol. *307*, G397–G409.

3. Russell, E.S., Nash, D.J., Bernstein, S.E., Kent, E.L., McFarland, E.C., Matthews, S.M., and Norwood, M.S. (1970). Characterization and genetic studies of microcytic anemia in house mouse. Blood *35*, 838–850.

4. Fleming, M.D., Trenor, C.C., 3rd, Su, M.A., Foernzler, D., Beier, D.R., Dietrich, W.F., and Andrews, N.C. (1997). Microcytic anaemia mice have a mutation in Nramp2, a candidate iron transporter gene. Nat. Genet. *16*, 383–386.

5. Sladic-Simic, D., Martinovitch, P.N., Zivkovic, N., Pavić, D., Martinovic, J., Kahn, M., and Ranney, H.M. (1969). A thalassemia-like disorder in Belgrade laboratory rats. Ann. N Y Acad. Sci. *165*, 93–99.

6. Fleming, M.D., Romano, M.A., Su, M.A., Garrick, L.M., Garrick, M.D., and Andrews, N.C. (1998). Nramp2 is mutated in the anemic Belgrade (b) rat: evidence of a role for Nramp2 in endosomal iron transport. Proc. Natl. Acad. Sci. USA *95*, 1148–1153.

7. Gunshin, H., Fujiwara, Y., Custodio, A.O., Direnzo, C., Robine, S., and Andrews, N.C. (2005). Slc11a2 is required for intestinal iron absorption and erythropoiesis but dispensable in placenta and liver. J. Clin. Invest. *115*, 1258–1266.

8. Garrick, L.M., Dolan, K.G., Romano, M.A., and Garrick, M.D. (1999). Non-transferrin-bound iron uptake in Belgrade and normal rat erythroid cells. J. Cell. Physiol. *178*, 349–358.

9. Canonne-Hergaux, F., and Gros, P. (2002). Expression of the iron transporter DMT1 in kidney from normal and anemic mk mice. Kidney Int. *62*, 147–156.

10. Shawki, A., Anthony, S.R., Nose, Y., Engevik, M.A., Niespodzany, E.J., Barrientos, T., Öhrvik, H., Worrell, R.T., Thiele, D.J., and Mackenzie, B. (2015). Intestinal DMT1 is critical for iron absorption in the mouse but is not required for the absorption of copper or manganese. Am. J. Physiol. Gastrointest. Liver Physiol. *309*, G635–G647.

11. Zhou, X.Y., Tomatsu, S., Fleming, R.E., Parkkila, S., Waheed, A., Jiang, J., Fei, Y., Brunt, E.M., Ruddy, D.A., Prass, C.E., et al. (1998). HFE gene knockout produces mouse model of hereditary hemochromatosis. Proc. Natl. Acad. Sci. USA *95*, 2492–2497.

12. Levy, J.E., Montross, L.K., and Andrews, N.C. (2000). Genes that modify the hemochromatosis phenotype in mice. J. Clin. Invest. *105*, 1209–1216.

13. Roetto, A., Papanikolaou, G., Politou, M., Alberti, F., Girelli, D., Christakis, J., Loukopoulos, D., and Camaschella, C. (2003). Mutant antimicrobial peptide hepcidin is associated with severe juvenile hemochromatosis. Nat. Genet. *33*, 21–22.

14. Sandhu, K., Flintoff, K., Chatfield, M.D., Dixon, J.L., Ramm, L.E., Ramm, G.A., Powell, L.W., Subramaniam, V.N., and Wallace, D.F. (2018). Phenotypic analysis of hemochromatosis subtypes reveals variations in severity of iron overload and clinical disease. Blood *132*, 101–110.

15. Xiao, B., and Merlin, D. (2012). Oral colon-specific therapeutic approaches toward treatment of inflammatory bowel disease. Expert Opin. Drug Deliv. *9*, 1393–1407.

16. Zhang, M., Wang, X., Han, M.K., Collins, J.F., and Merlin, D. (2017). Oral administration of ginger-derived nanolipids loaded with siRNA as a novel approach for efficient siRNA drug delivery to treat ulcerative colitis. Nanomedicine (Lond.) *12*, 1927–1943.

17. Zhang, M., Xu, C., Liu, D., Han, M.K., Wang, L., and Merlin, D. (2018). Oral delivery of nanoparticles loaded with ginger active compound, 6-shogaol, attenuates ulcerative colitis and promotes wound healing in a murine model of ulcerative colitis. J. Crohn's Colitis *12*, 217–229.

18. Zhang, M., Collins, J.F., and Merlin, D. (2016). Do ginger-derived nanoparticles represent an attractive treatment strategy for inflammatory bowel diseases? Nanomedicine (Lond.) *11*, 3035–3037.

19. Mu, J., Zhuang, X., Wang, Q., Jiang, H., Deng, Z.B., Wang, B., Zhang, L., Kakar, S., Jun, Y., Miller, D., and Zhang, H.G. (2014). Interspecies communication between plant and mouse gut host cells through edible plant derived exosome-like nanoparticles. Mol. Nutr. Food Res. *58*, 1561–1573.

20. Zhang, M., Viennois, E., Xu, C., and Merlin, D. (2016). Plant derived edible nanoparticles as a new therapeutic approach against diseases. Tissue Barriers *4*, e1134415.

21. Wang, Q., Ren, Y., Mu, J., Egilmez, N.K., Zhuang, X., Deng, Z., Zhang, L., Yan, J., Miller, D., and Zhang, H.G. (2015). Grapefruit-derived nanovectors use an activated leukocyte trafficking pathway to deliver therapeutic agents to inflammatory tumor sites. Cancer Res. *75*, 2520–2529.

22. Wang, Q., Zhuang, X., Mu, J., Deng, Z.B., Jiang, H., Zhang, L., Xiang, X., Wang, B., Yan, J., Miller, D., and Zhang, H.G. (2013). Delivery of therapeutic agents by nanoparticles made of grapefruit-derived lipids. Nat. Commun. *4*, 1867.

23. Ganz, T. (2018). Erythropoietic regulators of iron metabolism. Free Radic. Biol. Med. Published online July 5, 2018. https://doi.org/10.1016/j.freeradbiomed.2018.07.003.

24. Lesbordes-Brion, J.C., Viatte, L., Bennoun, M., Lou, D.Q., Ramey, G., Houbron, C., Hamard, G., Kahn, A., and Vaulont, S. (2006). Targeted disruption of the hepcidin 1 gene results in severe hemochromatosis. Blood *108*, 1402–1405.

25. Zhang, M., Viennois, E., Prasad, M., Zhang, Y., Wang, L., Zhang, Z., Han, M.K., Xiao, B., Xu, C., Srinivasan, S., and Merlin, D. (2016). Edible ginger-derived nanoparticles: a novel therapeutic approach for the prevention and treatment of inflammatory bowel disease and colitis-associated cancer. Biomaterials *101*, 321–340.

26. Garrick, M.D., Kuo, H.C., Vargas, F., Singleton, S., Zhao, L., Smith, J.J., Paradkar, P., Roth, J.A., and Garrick, L.M. (2006). Comparison of mammalian cell lines expressing distinct isoforms of divalent metal transporter 1 in a tetracycline-regulated fashion. Biochem. J. *398*, 539–546.

27. Qiu, A., Jansen, M., Sakaris, A., Min, S.H., Chattopadhyay, S., Tsai, E., Sandoval, C., Zhao, R., Akabas, M.H., and Goldman, I.D. (2006). Identification of an intestinal folate transporter and the molecular basis for hereditary folate malabsorption. Cell *127*, 917–928.

28. Roger, E., Kalscheuer, S., Kirtane, A., Guru, B.R., Grill, A.E., Whittum-Hudson, J., and Panyam, J. (2012). Folic acid functionalized nanoparticles for enhanced oral drug delivery. Mol. Pharm. *9*, 2103–2110.

29. Thomas, C., and Thomas, L. (2002). Biochemical markers and hematologic indices in the diagnosis of functional iron deficiency. Clin. Chem. *48*, 1066–1076.

30. Addison, G.M., Beamish, M.R., Hales, C.N., Hodgkins, M., Jacobs, A., and Llewellin, P. (1972). An immunoradiometric assay for ferritin in the serum of normal subjects and patients with iron deficiency and iron overload. J. Clin. Pathol. *25*, 326–329.

31. Ferguson, C.J., Wareing, M., Ward, D.T., Green, R., Smith, C.P., and Riccardi, D. (2001). Cellular localization of divalent metal transporter DMT-1 in rat kidney. Am. J. Physiol. Renal Physiol. *280*, F803–F814.

32. Wareing, M., Ferguson, C.J., Green, R., Riccardi, D., and Smith, C.P. (2000). In vivo characterization of renal iron transport in the anaesthetized rat. J. Physiol. *524*, 581–586.

33. Veuthey, T., Hoffmann, D., Vaidya, V.S., and Wessling-Resnick, M. (2014). Impaired renal function and development in Belgrade rats. Am. J. Physiol. Renal Physiol. *306*, F333–F343.

34. Bardou-Jacquet, E., Island, M.L., Jouanolle, A.M., Détivaud, L., Fatih, N., Ropert, M., Brissot, E., Mosser, A., Maisonneuve, H., Brissot, P., and Loréal, O. (2011). A novel N491S mutation in the human SLC11A2 gene impairs protein trafficking and in association with the G212V mutation leads to microcytic anemia and liver iron overload. Blood Cells Mol. Dis. *47*, 243–248.

35. Beaumont, C., Delaunay, J., Hetet, G., Grandchamp, B., de Montalembert, M., and Tchernia, G. (2006). Two new human DMT1 gene mutations in a patient with microcytic anemia, low ferritinemia, and liver iron overload. Blood *107*, 4168–4170.

36. Lam-Yuk-Tseung, S., Camaschella, C., Iolascon, A., and Gros, P. (2006). A novel R416C mutation in human DMT1 (SLC11A2) displays pleiotropic effects on function and causes microcytic anemia and hepatic iron overload. Blood Cells Mol. Dis. *36*, 347–354.

37. Lam-Yuk-Tseung, S., Mathieu, M., and Gros, P. (2005). Functional characterization of the E399D DMT1/NRAMP2/SLC11A2 protein produced by an exon 12 mutation in a patient with microcytic anemia and iron overload. Blood Cells Mol. Dis. *35*, 212–216.

38. Mims, M.P., Guan, Y., Pospisilova, D., Priwitzerova, M., Indrak, K., Ponka, P., Divoky, V., and Prchal, J.T. (2005). Identification of a human mutation of DMT1 in a patient with microcytic anemia and iron overload. Blood *105*, 1337–1342.

39. Priwitzerova, M., Nie, G., Sheftel, A.D., Pospisilova, D., Divoky, V., and Ponka, P. (2005). Functional consequences of the human DMT1 (SLC11A2) mutation on protein expression and iron uptake. Blood *106*, 3985–3987.

40. Iolascon, A., d'Apolito, M., Servedio, V., Cimmino, F., Piga, A., and Camaschella, C. (2006). Microcytic anemia and hepatic iron overload in a child with compound heterozygous mutations in DMT1 (SCL11A2). Blood *107*, 349–354.

41. Parmar, J.H., Davis, G., Shevchuk, H., and Mendes, P. (2017). Modeling the dynamics of mouse iron body distribution: hepcidin is necessary but not sufficient. BMC Syst. Biol. *11*, 57.

42. Chappelle, E., Gabrio, B.W., Stevens, A.R., Jr., and Finch, C.A. (1955). Regulation of body iron content through excretion in the mouse. Am. J. Physiol. *182*, 390–392.

43. Liuzzi, J.P., Aydemir, F., Nam, H., Knutson, M.D., and Cousins, R.J. (2006). Zip14 (Slc39a14) mediates non-transferrin-bound iron uptake into cells. Proc. Natl. Acad. Sci. USA *103*, 13612–13617.

44. Wang, C.Y., Jenkitkasemwong, S., Duarte, S., Sparkman, B.K., Shawki, A., Mackenzie, B., and Knutson, M.D. (2012). ZIP8 is an iron and zinc transporter whose cell-surface expression is up-regulated by cellular iron loading. J. Biol. Chem. *287*, 34032–34043.

45. Eide, D.J. (2004). The SLC39 family of metal ion transporters. Pflugers Arch. *447*, 796–800.

46. Clarke, L.L. (2009). A guide to Ussing chamber studies of mouse intestine. Am. J. Physiol. Gastrointest. Liver Physiol. *296*, G1151–G1166.

47. Lynch, S.R., Skikne, B.S., and Cook, J.D. (1989). Food iron absorption in idiopathic hemochromatosis. Blood *74*, 2187–2193.

48. Hunt, J.R., and Zeng, H. (2004). Iron absorption by heterozygous carriers of the HFE C282Y mutation associated with hemochromatosis. Am. J. Clin. Nutr. *80*, 924–931.

49. Brissot, P., Troadec, M.B., and Loréal, O. (2004). Intestinal absorption of iron in HFE-1 hemochromatosis: local or systemic process? J. Hepatol. *40*, 702–709.

50. Zhang, H., Ameen, N., Melvin, J.E., and Vidyasagar, S. (2007). Acute inflammation alters bicarbonate transport in mouse ileum. J. Physiol. *581*, 1221–1233.

51. Yin, L., Vijaygopal, P., Menon, R., Vaught, L.A., Zhang, M., Zhang, L., Okunieff, P., and Vidyasagar, S. (2014). An amino acid mixture mitigates radiation-induced gastrointestinal toxicity. Health Phys. *106*, 734–744.

52. Zhang, K., Yin, L., Zhang, M., Parker, M.D., Binder, H.J., Salzman, P., Zhang, L., Okunieff, P., and Vidyasagar, S. (2011). Radiation decreases murine small intestinal HCO3- secretion. Int. J. Radiat. Biol. *87*, 878–888.

53. Ha, J.H., Doguer, C., Flores, S.R.L., Wang, T., and Collins, J.F. (2018). Progressive increases in dietary iron are associated with the emergence of pathologic disturbances of copper homeostasis in growing rats. J. Nutr. *148*, 373–378.

54. Ha, J.H., Doguer, C., Wang, X., Flores, S.R., and Collins, J.F. (2016). High-iron consumption impairs growth and causes copper-deficiency anemia in weanling Sprague-Dawley rats. PLoS ONE *11*, e0161033.

55. Gulec, S., and Collins, J.F. (2013). Investigation of iron metabolism in mice expressing a mutant Menke's copper transporting ATPase (Atp7a) protein with diminished activity (Brindled; Mo (Br) (/y)). PLoS ONE *8*, e66010.

56. Reeves, P.G., Nielsen, F.H., and Fahey, G.C., Jr. (1993). AIN-93 purified diets for laboratory rodents: final report of the American Institute of Nutrition ad hoc writing committee on the reformulation of the AIN-76A rodent diet. J. Nutr. *123*, 1939–1951.

57. Gunshin, H., Allerson, C.R., Polycarpou-Schwarz, M., Rofts, A., Rogers, J.T., Kishi, F., Hentze, M.W., Rouault, T.A., Andrews, N.C., and Hediger, M.A. (2001). Iron-dependent regulation of the divalent metal ion transporter. FEBS Lett. *509*, 309–316.

58. Fleming, R.E., Migas, M.C., Zhou, X., Jiang, J., Britton, R.S., Brunt, E.M., Tomatsu, S., Waheed, A., Bacon, B.R., and Sly, W.S. (1999). Mechanism of increased iron absorption in murine model of hereditary hemochromatosis: increased duodenal expression of the iron transporter DMT1. Proc. Natl. Acad. Sci. USA *96*, 3143–3148.

59. Moretti, D., van Doorn, G.M., Swinkels, D.W., and Melse-Boonstra, A. (2013). Relevance of dietary iron intake and bioavailability in the management of HFE hemochromatosis: a systematic review. Am. J. Clin. Nutr. *98*, 468–479.

60. Gulec, S., and Collins, J.F. (2014). Silencing the Menkes copper-transporting ATPase (Atp7a) gene in rat intestinal epithelial (IEC-6) cells increases iron flux via transcriptional induction of ferroportin 1 (Fpn1). J. Nutr. *144*, 12–19.

YMTHE, Volume *27*

Supplemental Information

Oral Gavage of Ginger Nanoparticle-Derived Lipid Vectors Carrying Dmt1 siRNA Blunts Iron Loading in Murine Hereditary Hemochromatosis

Xiaoyu Wang, Mingzhen Zhang, Shireen R.L. Flores, Regina R. Woloshun, Chunhua Yang, Liangjie Yin, Ping Xiang, Xiaodong Xu, Michael D. Garrick, Sadasivan Vidyasagar, Didier Merlin, and James F. Collins

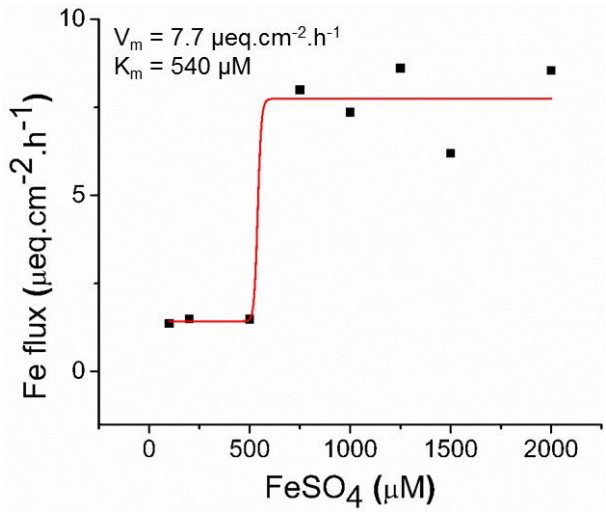

Figure S1. Transepithelial iron transport at different iron concentrations at pH 7.4 in WT mice. Ussing chambers were utilized to assess transepithelial Fe flux. Duodenal epithelial sheets from adult 129S6 male mice were used to determine the optimal $FeSO_4$ concentration. Data represent Fe flux at 100, 200, 500, 750, 1000, 1250, 1500 and 2000 µM $FeSO_4$ (n = 3).

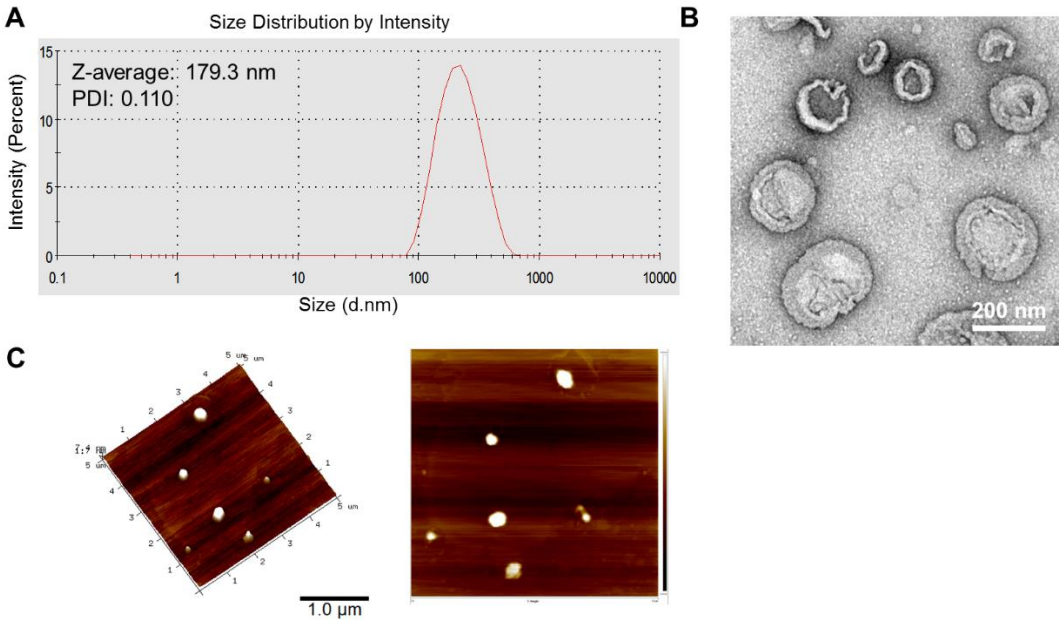

Figure S2. Characterization of ginger nanoparticle-derived lipid vector (GDLVs). GDLVs were measured by dynamic light scattering (DLS) (**A**), and visualized by transmission electron microscopy (TEM) (**B**) and atomic force microscopy (AFM) (**C**).

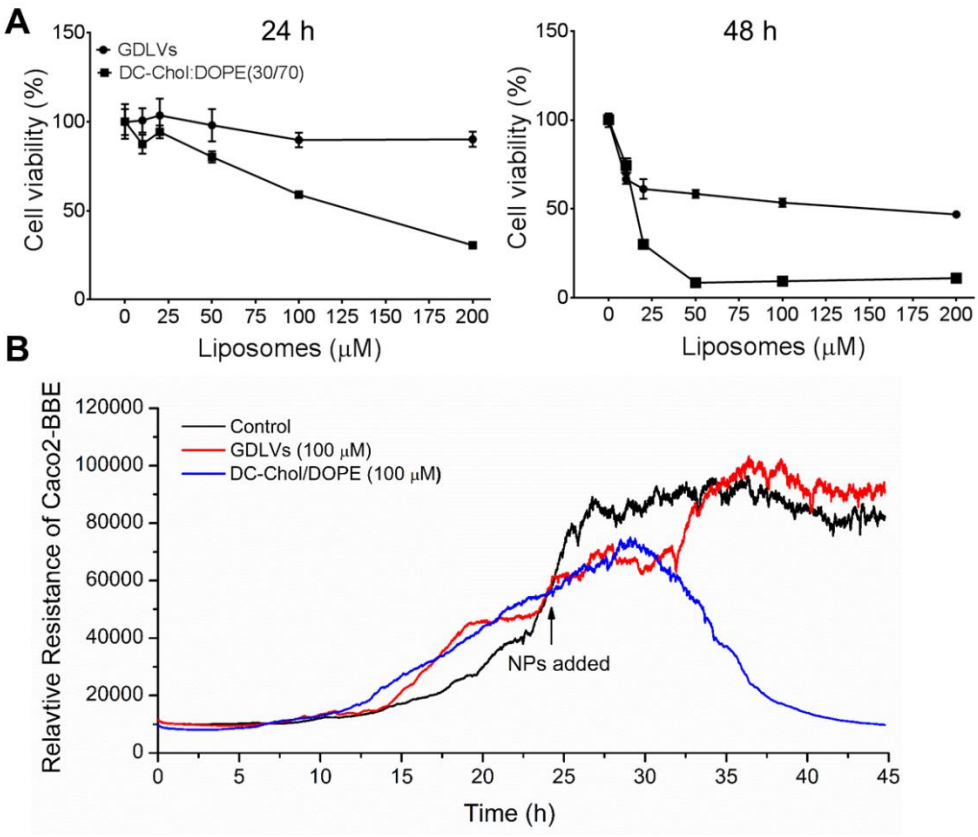

Figure S3. Biocompatibility of GDLVs. Colon-26 cell viability was measured by MTT assay after 24- or 48-hours exposure to GDLVs or commercial DC-Chol/DOPE liposomes (**A**). Electrical cell-substrate impedance sensing (ECIS) was used to monitor real-time barrier function (permeability) of Caco2-BBE cell monolayers (**B**). This image is representative of 4 identical experiments conducted.

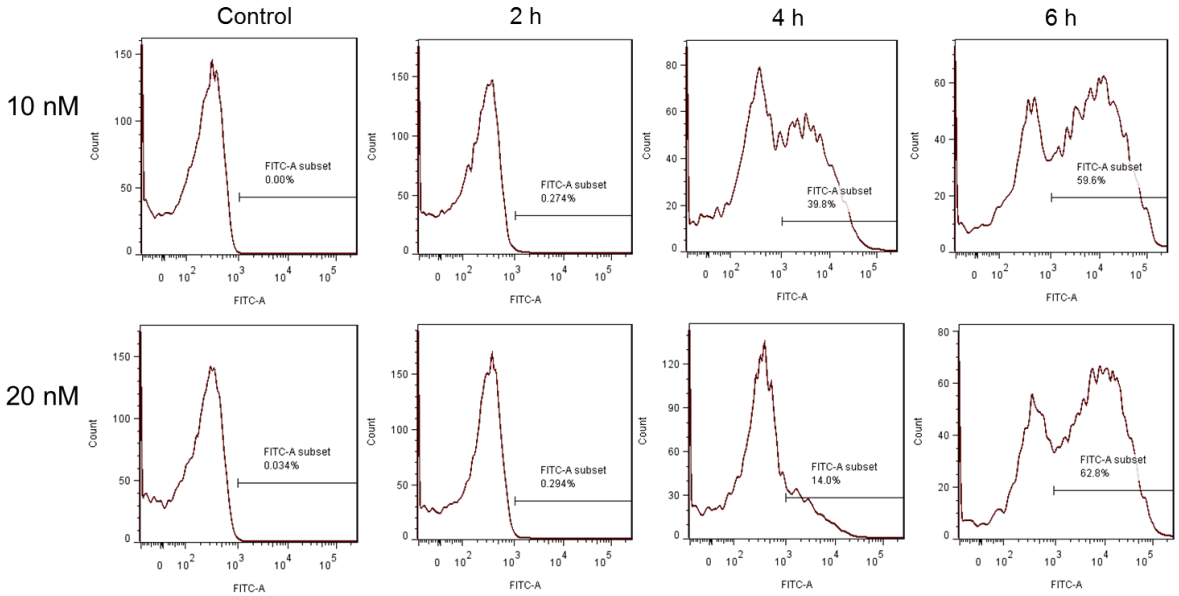

Figure S4. Cellular uptake of GDLVs/siRNA in Colon-26 cells measured by flow cytometry. Cellular uptake of GDLVs/siRNA in Colon-26 cells after 2, 4 or 6 hours. Colon-26 cells were treated with GDLVs-siRNA-FITC at 10 nM and 20 nM. The cell uptake efficiency was quantified by flow cytometry by gating for FITC fluorescence.

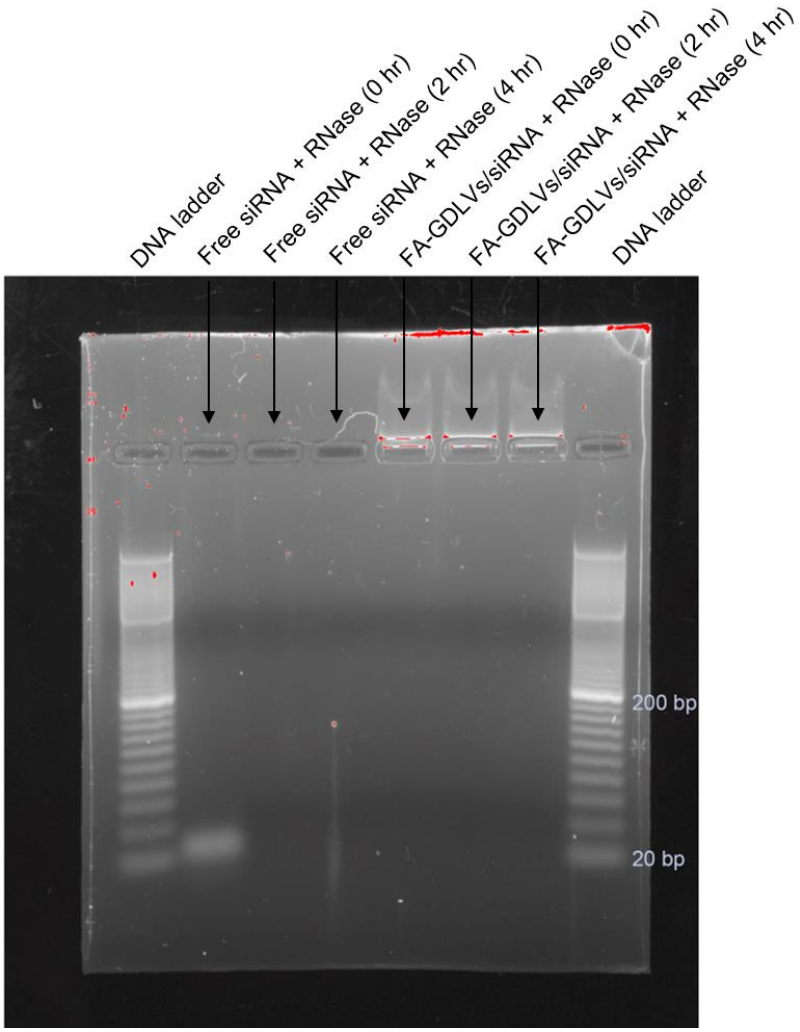

Figure S5. Stability of FA-GDLVs/siRNA. Free siRNA (10 μM) and FA-GDLVs/siRNA (10 μM) were treated with 10 μg/mL RNase (Sigma, cat#R-6513) for 0, 2, and 4hr. DNA ladder (Sigma, cat# p1598) was used as marker. 2% Agarose gel with 0.01%GelRed Nucleic Acid dye in TAE, running buffer: TAE; 110v, 40.0 min; loading volume: 10 μL (8 μL sample mixed with 2 μL RNA loading dye).

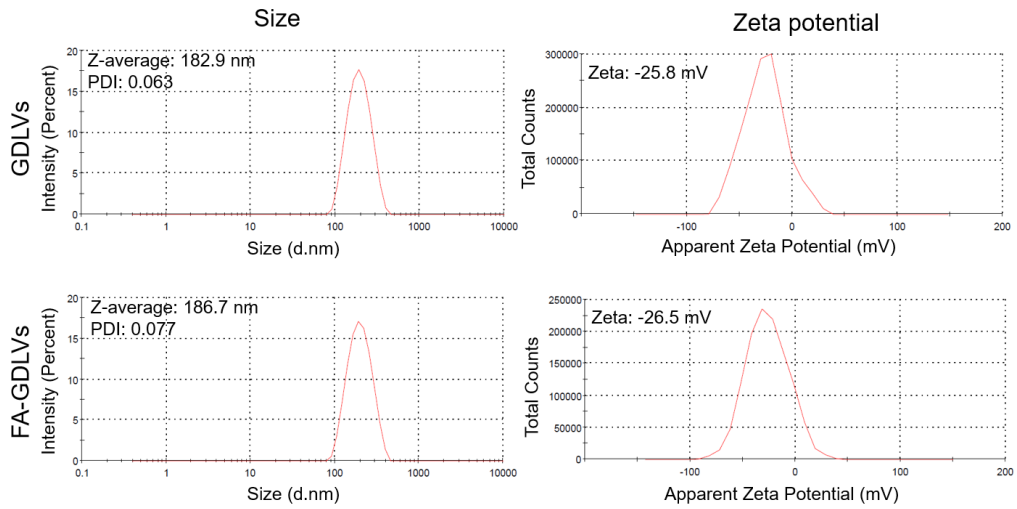

Figure S6. Characterization and comparison of GDLVs and FA-GDLVs. Size and zeta potentials of GDLV and FA-GDLVs were measured by dynamic light scattering (DLS).

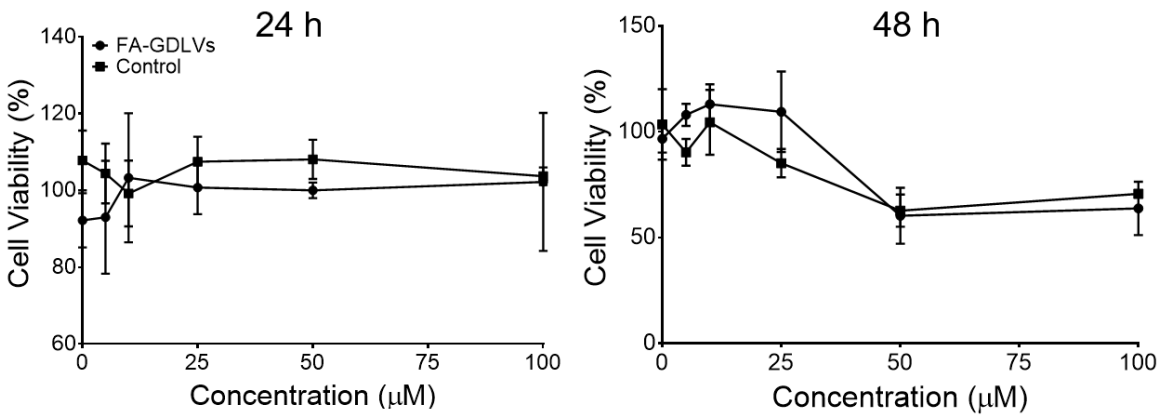

Figure S7. Biocompatibility of FA-GDLVs. Colon-26 cell viability was measured by MTT assay after 24- or 48-hours exposure to FA-GDLVs or control (PBS). FA-GDLVs did not show growth inhibition compared to the control groups. There is thus no IC_{50} value for FA-GDLVs up to 100 µM (n=4).

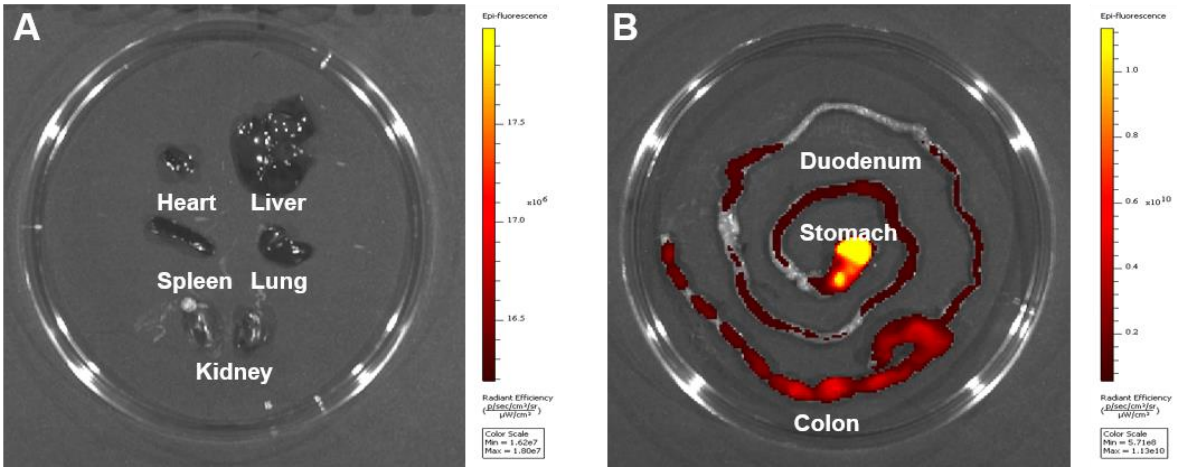

Figure S8. Biodistribution of FA-GDLVs. Mice (n=5) were fasted for 4 hours before gavage and images were captured by an IVIS series preclinical *in vivo* imaging system (Perkin Elmer; MA, USA) 4h post-gavage. Concentration of FA-GDNVs was 1 mg/mL; concentration of labeling dye (DiR) was 10uM; gavage volume was 0.1 mL. A. An image of organs (heart, liver, spleen, lung and kidney) (**A**). An image of the whole gut (**B**). Representative images are shown.

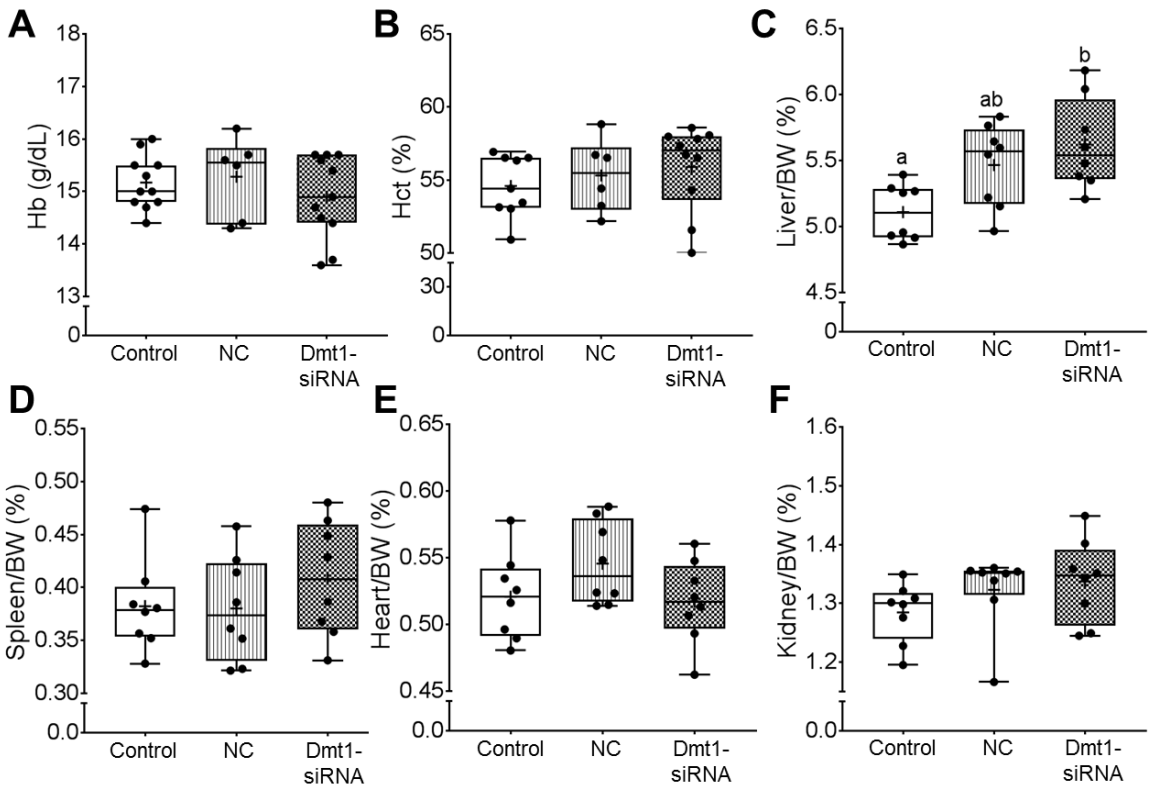

Figure S9. Hb concentrations and tissue weights of Hepc$^{-/-}$ mice treated with FA-GDLVs loaded with Dmt1 siRNA. Female Hepc$^{-/-}$ mice (19 days old) were orally gavaged daily for 16 days with saline (control), negative control-siRNA (NC) or Dmt1-siRNA FA-GDLVs. Mice were fed a low-iron diet on days 9-16. Shown are Hb levels (A), Hct levels (B), and relative liver (**C**), spleen (**D**), heart (**E**) and kidney weights (**F**). Data were analyzed by one-way ANOVA and are presented a box plots for n = 6-11 mice per group. Groups labeled with different letters are statistically different from one another (C).

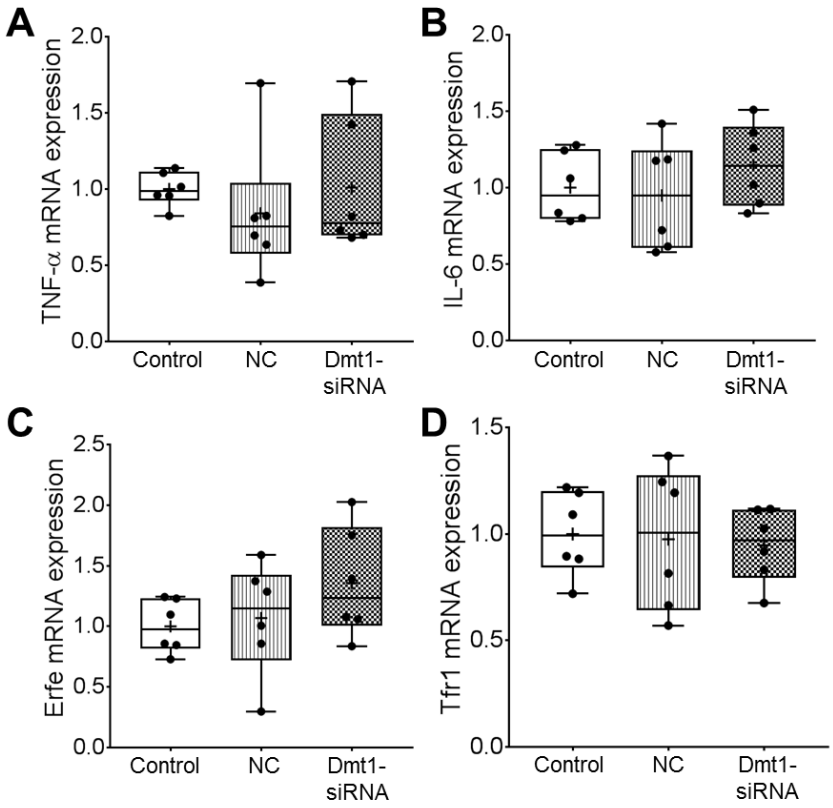

Figure S10. Hepatic TNF-α and IL-6, and bone marrow Erfe and Tfr1, mRNA expression in Hepc$^{-/-}$ mice was not affected by administration of FA-GDLVs loaded with Dmt1 siRNA. Female Hepc$^{-/-}$ mice (19 days old) were orally gavaged daily for 16 days with saline (control), negative control-siRNA (NC) or Dmt1-siRNA FA-GDLVs. Mice were fed a low-iron diet on days 9-16. Shown are TNF-α (**A**) and IL-6 (**B**) mRNA expression in liver, and Erfe (**C**) and Tfr1 (**D**) mRNA expression in bone marrow, which were normalized to expression of CypA. Data were analyzed by one-way ANOV A and are presented a box plots for n = 6 mice per group.

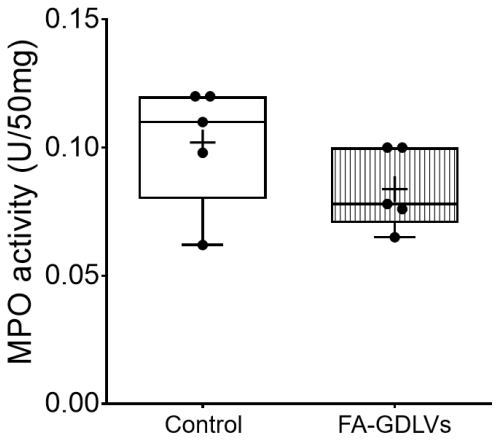

Figure S11. MPO activity in duodenum of FA-GDLVs-treated mice. Mice were gavaged with saline (control) or FA-GDLVs, and then 4 hours later, mice were euthanized and duodenal scrapes were collected for the assay (n=5/group).

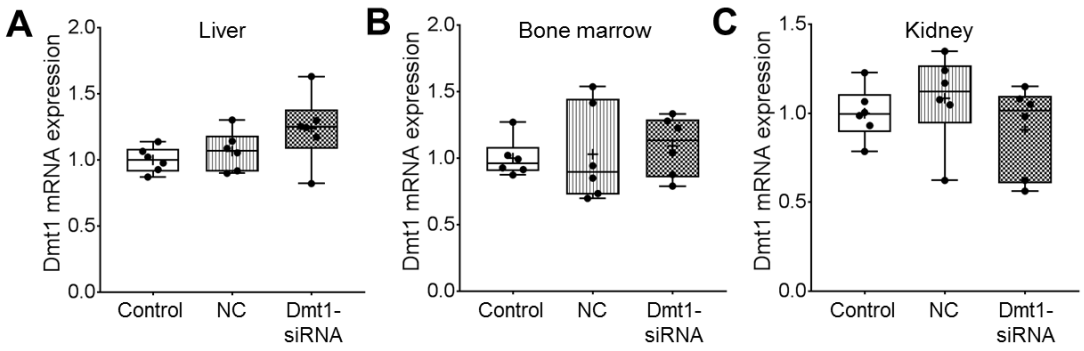

Figure S12. Dmt1 mRNA expression in liver, bone marrow and kidney of Hepc$^{-/-}$ mice was not affected by administration of FA-GDLVs loaded with Dmt1 siRNA. Female Hepc$^{-/-}$ mice (19 days old) were orally gavaged daily for 16 days with saline (control), negative control-siRNA (NC) or Dmt1-siRNA FA-GDLVs. Mice were fed a low-iron diet on days 9-16. Dmt1 mRNA expression in liver (**A**), bone marrow (**B**) and kidney (**C**) was normalized to expression of CypA. Data were analyzed by one-way ANOVA (with no significant changes noted) and are presented as box plots for n=6 mice/group.

Constituent, mM	pH 5.0	pH 6.5	pH 7.4
Na^+	119.6	140.4	144.5
K^+	5.2	5.2	5.2
Mg^{2+}	1.2	1.2	1.2
Ca^{2+}	1.2	1.2	1.2
Acetate	50	—	—
Cl^-	74	115	115
Citrate	25	25	25
$H_2PO_4^-$	—	7.6	3.5
HPO_4^{2-}	—	1.4	5.5

Table S1. Composition of experimental buffers. Different buffer systems were chosen based on their pKa that was best suited or closer to the pH of the buffer solution used for the studies. Henderson-Hasselbalch equation was used to calculate the ratio of acid and its corresponding conjugate base. The buffers were then titrated using 1N HCl to confirm the buffering capacity and arrive at the titration curve. The stability of the buffer with time was determined by measuring the pH at 25^{o}C at regular interval for 24 hours. The final osmolarity of the solution was 296mOsms.

Transcript	Forward (5’ to 3’)	Reverse (5’ to 3’)
Dmt1	GTGATCCTGACCCGGTCTATCG	TGAGGATGGGTATGAGAGCAAAGG
Epo	ATGAAGACTTGCAGCGTGGA	AGGCCCAGAGGAATCAGTAG
Erfe	ACTCACCAAGCAGCCAAGAA	TTCTCCAGCCCCATCACAGT
TNF-α	CACAAGATGCTGGGACAGTGA	TCCTTGATGGTGGTGCATGA
IL-6	CTGCAAGAGACTTCCATCCAGTT	AGGGAAGGCCGTGGTTGT
Tfr1	AACTTACCCATGACGTTGATTGAACC	ACAGCCACTGTAGACTTAGACCCATATC
CypA	CTTACGACAAGCAGCCCTTCATG	AGCTGTTTTTAACTCACTGCTGTTGTA

Table S2. Primer Sequences